Technical Memorandum 33-630

Testing and Evaluation of the LES-6 Pulsed Plasma Thruster by Means of a Torsion Pendulum System

J. P. Hamidian

J. B. Dahlgren

Technical Memorandum 33-630

Testing and Evaluation of the LES-6 Pulsed Plasma Thruster by Means of a Torsion Pendulum System

J. P. Hamidian

J. B. Dahlgren

PREFACE

The work described in this report was performed by the Guidance and
Control Division of the Jet Propulsion Laboratory.

CONTENTS

CONTENTS (contd)

TABLES

FIGURES

CONTENTS (contd)

CONTENTS (contd)

ABSTRACT

Performance characteristics of the LES-6 pulsed plasma thruster over a range of input conditions were investigated by means of a torsion pendulum system. Parameters of particular interest included the impulse bit and time average thrust (and their repeatability), specific impulse, mass ablated per discharge, specific thrust, energy per unit area, efficiency, and variation of performance with ignition command rate. Intermittency of the thruster as affected by input energy and igniter resistance were also investigated. Comparative experimental data from the Massachusetts Institute of Technology and from the National Aeronautics and Space Administration's Goddard Space Flight Center have shown good correlation with the data presented.

The results of these tests indicate that the LES-6 thruster, with some identifiable design improvements, represents an attractive reaction control thruster for attitude control applications on long-life spacecraft requiring small metered impulse bits for precise pointing control of science instruments.

I. INTRODUCTION

Under the auspices of the Aero Propulsion Laboratory of the United States Air Force, research work was performed by the Republic Aviation Division of the Fairchild Hiller Corporation from 1967 to 1968 and directed toward the improvement of pulsed plasma technology. This work resulted in the design and development of a valveless solid propellant pulsed plasma microthruster having a high level of reliability and a passive failure mode (Ref. 1). The microthruster was subsequently used successfully in 1968 on the LES-6 station keeping satellite of the Massachusetts Institute of Technology (MIT) Lincoln Laboratory. Pulsed plasma microthrusters aimed at potential attitude control applications on long-duration missions have been under development intermittently at the Jet Propulsion Laboratory (JPL) since about 1965. Some of the most challenging aspects of microthruster technology involve the development of techniques for measuring the extremely low thrust levels produced by low-energy pulsed plasma thrusters. The major portion of the JPL effort in the fiscal year 1972 was devoted to the design and development of the test techniques and hardware. The task in fiscal year 1973 consisted of data collection, performance and data analysis, and the comparison of data with those obtained by MIT and the Goddard Space Flight Center (GSFC).

The objectives of this part of the program were:

(1)   Development of a torsion pendulum system, the necessary test equipment, and test techniques for evaluating thrusters with thrust levels in the micronewton (micropound) ranges.

(2)   Initiation of a test program for evaluating specific performance parameters (specific impulse, efficiency, impulse bit, time average thrust, and specific thrust) of the LES-6 thruster.

(3) Analysis and study of available test data and relationships between the input and the output parameters of a LES-6 thruster. Assessment and applicability of the LES-6 thrusters as the thrust actuators within an attitude control system of a spacecraft.

II. THE LES-6 THRUSTER AND ITS OPERATION

A LES-6 thruster is schematized in Fig. 1; it consists of a solid virgin Teflon fuel bar which is fed continuously between two electrodes by means of a Negator spring. A spark plug is located at the edge of the propellant rod. The electrodes are connected to the main discharge capacitor and the spark plug is connected to the initiating capacitor. The main discharge capacitor is charged to its operating voltage prior to an ignition. Upon receiving an ignition command signal from an external source, the initiating capacitor discharges between the cathode and the spark plug. This micro-discharge from a small initiating capacitor closes an electric circuit which allows the main discharge capacitor to discharge without requiring an additional switching system. The main discharge depolymerizes and removes material from the exposed surface of the Teflon propellant rod and produces thrust by discharging it electromagnetically and gasdynamically through the thruster nozzle.

A LES-6 thruster assembly consists of two thrusters and one main discharge capacitor. Each thruster has a separate ignition capacitor and ignition circuit. The LES-6 thruster is designed to operate in either a single- or dual-thruster mode.

Due to the low thrust level characteristics of the LES-6-type solid propellant pulsed plasma thruster, an extremely sensitive torsion pendulum system was required for the evaluation. A torsion pendulum thrust stand, originally developed by General Electric for evaluation of a waxy propellant pulsed plasma thruster, was modified for the investigation (Ref. 2). The torsion pendulum assembly itself consisted of three major elements: a torsion wire, a pendulum platform, and the supporting structure.

The torsion wire is clamped at one end to the supporting structure and at the other end to the platform. The torsion wire is used both as the torsional responding element and as a lead to the input voltage network on the

platform. The thruster is mounted at one end of the platform so that the thrust vector is normal to the radial axis of the platform. A shadow plate mechanism parallel to the thrust vector is part of the platform. The platform is balanced by the counter weight of the thruster positioned on the platform and 180 deg away from the thruster itself.

The supporting structure is equipped with threaded adjustable legs, a rotating adjustable clamp at the top, and an angular readout protractor positioned at the same elevation as the shadow plate. Photographs of the torsion pendulum system are shown in Figs. 2 and 3.

A functional block diagram of the torsion pendulum system is shown in Fig. 4. The voltage dividing network is designed to receive high-voltage input via the torsion wire, charging both the main discharge capacitor and the ignition capacitor of the thruster. Upon receiving an ignition command signal from the trigger generating network via the optical coupler, the thruster discharges, producing thrust proportional to the rate of the ignition command signal and the energy stored in the main discharge capacitor. The pendulum system responds to the generated thrust impulse by its angular displacement. The shadow bar mechanism of the pendulum, along with an optical coupling subsystem, allows the system to measure this angular displacement and record it both on an X-Y plotter and on a digital voltmeter.

Since the pendulum system is critically damped, the output thrust causes the pendulum to be displaced to some maximum displacement angle and to sustain this angle irrespective of the total number of input pulses. Figure 5 represents a typical time average thrust response of the torsional pendulum system to the output thrust of the LES-6 thruster. The thrust value is calculated from Eqs. (1) and (2):

$$\Delta\theta = E_o/C \tag{1}$$

$$F = \frac{\Delta\theta K}{R} \text{ in micronewtons (micropounds)} \tag{2}$$

where

$\Delta\theta$ = displacement angle in degrees

K = spring constant in μN-m/deg (μlb-ft/deg)

R = arm radius, m (ft), at which the thruster is mounted from the torsion wire

C = scale factor of the photosensing subsystem in mv/deg

E_o = output voltage from photosensing subsystem in mv.

F = the thrust value in micronewtons (micropounds)

The accumulative input pulses of each run, photosensor output voltage, ignition command rate, and vacuum level of the system are continuously recorded as reference parameters. Subsystem circuit diagrams are shown in Appendix A (Figs. A-1 through A-4).

III. CALIBRATION AND SUBSYSTEMS EVALUATIONS

The following subsystem tests and calibrations were made before the torsional pendulum system was assembled.

The torsional pendulum torsion wire was selected on the basis of experiments performed with various gages and types of torsion wires. Strain data indicated that 0.41-mm (16-mil) stainless steel music wire was capable of adequately supporting the platform equipment (3.63 kg = 8 lb) and responding to the low thrust level of the thruster. Strain data for this selected torsion wire is shown in Table A-1 of Appendix A. The torsion wire was preloaded with a 9.07-kg (20-lb) load prior to its application and its calibration. A standard inertia disk was used to obtain the spring constant of the torsion wire at a vacuum level of 133.3×10^{-5} N/m^2 (1×10^{-5} torr). (Views of the standard inertia disk are shown in Fig. A-4 of Appendix A.) The spring constant was calculated from Eq. (3):

$$K = 0.93 \frac{I_c}{T^2} \times 10^6 \qquad (3)$$

where

I_c = moment of inertia of the standard inertia disk in kg-m^2 (slug-ft^2)

T = period of oscillation for a complete cycle of the pendulum in seconds

K = torsion wire spring constant in μN-m/deg (μlb-ft/deg)

The period of oscillation of the pendulum system with the standard inertia disk was measured with the torsion pendulum assembly under 133.3×10^{-5} N/m^2 (1×10^{-5} torr) of vacuum. The results of the experiment (see Table A-2 of Appendix A) show that the average period of oscillation over 10 cycles for vacuum condition was calculated to be 43.26 s. The values of both T and I_c (see Appendix B) were substituted into Eq. (3), and the spring constant of the wire was calculated to be 8.05 μN-m/deg (5.915-μlb-ft/deg).

Sensors were added to the system so that the temperature rises of both the torsion wire and the voltage-dividing network could be measured. It was determined that these temperature rises were negligible.

An optical dividing head was used to calibrate the readout photosensor at ambient illumination. The result of the above experiment is shown in Table A-3 of Appendix A. Since the photosensor is used under the bell jar of the vacuum system, it was then recalibrated under the bell jar assembly, and a scale factor of 0.00635 millivolts per arc minute of the pendulum's displacement angle over a 3-deg range was obtained. Table A-4 of Appendix A is the result of this calibration.

A number of mechanical and electrical problems, which required correction, were experienced with the pendulum system, as discussed below.

A major problem was the pendulum's vibrational motions, which were found to be attributable to several sources, the chief one being the vacuum system's mechanical pump. The pump was removed and isolated from the pendulum system, and thus its effect was eliminated.

Another vibrational motion resulted from the vertical noncoincidence of the thrust axis and the pendulum's center of gravity. To correct this problem, the thruster counter's balance weight was aligned with the center line of the thruster nozzle, eliminating the vibrational motion of the platform which occurred during thrust impulse.

Electrical arcing was observed at several locations on the pendulum platform assembly and at the high-voltage feedthrough into the vacuum system bell jar. To eliminate the high-voltage arcing problem at the feedthrough connector, the Bendix connector was replaced with a pair of ceramic high-voltage feedthroughs with greater separation than the Bendix connector. The voltage-dividing network was reassembled in double-deck configuration and installed along with a shield on top of the thruster. This modification removed and shielded the voltage-dividing network power resistors from the thrust path and eliminated arcing from this area. The arcing at the thruster's input connectors was eliminated by installing side cover plates on the thruster.

To restrain the continuous oscillatory motion of the pendulum system, a critical damping mechanism was added. Based on the results of experiments with various damping fluids, Dow Corning DC-200 fluid, having a viscosity of $1 \times 10^{-3} m^2/s$ (1000 cs), was selected. The desired critical damping was achieved by immersing an approximate area of $0.968 cm^2$ ($0.15 in.^2$) of the pendulum paddle into the fluid.

IV. TEST CONFIGURATION AND TEST PROCEDURE

The torsion pendulum system, along with its supporting structure, was assembled into the Veeco 775 vacuum system. The vacuum system's roughing pump is rated at $42.5 cm^3/min$ ($15 ft^3/min$) while its diffusion pump is rated at $2000 cm^3/s$ ($70.7 ft^3/s$). The base diameter of the bell jar is 55.72 cm (18 in.) and its height is 76.2 cm (30.0 in.). The thruster is mounted on the platform so that the clearance between the nozzle of the thruster and the bell jar is approximately 6.35 cm (2.5 in.). Through various experiments, it was determined that the vacuum system would require approximately 2 h stabilization prior to any thrust measurement. Based on the above finding, a minimum 2-h stabilization period was allowed between two consecutive thrust measurements. All the subsystems and the components were tested individually, and the entire system was checked out for proper operation.

Among several parameters of interest, the input voltage of the main discharge capacitor was displayed on an oscilloscope at various voltages and pulse rates. The voltage-dividing network had a time-constant which allowed the main discharge capacitor to charge to approximately the applied voltage for pulse rates up to 3 pulses/s.

6

During thrust measurements, the vacuum level was kept at 600.4×10^{-6} N/m^2 (4.5×10^{-6} torr) and the experiments were conducted at ambient temperature.

A. Thrust Measurement and Available Data

The time average thrust measurement was initiated at various voltages and ignition command rates. Thrust data were averaged over 12 min continuous pulsing of the thruster. At a fixed ignition command rate, the main discharge voltage was varied at 50-V dc steps, and the time average thrust values were measured and recorded as in Table 1. During these experiments the igniter resistance and the area of the Teflon bar were not measured (except at 1 pulse/s). During the experiments, it was observed that the thruster misfired at 600 V dc of the main discharge voltage and it was nonoperative at 550 V dc.

B. Input Energy of the Main Discharge Capacitor and Impulse Bit

From the available test data, the corresponding average impulse bit of each energy level was computed and plotted as in Fig. 6. As can be seen from Fig. 6, the impulse bit is linearly dependent on the input energy. It can also be noted that the thruster requires a minimum of 0.25 joules of input energy to start firing. The 0.25-joule interception point has been verified experimentally by noting that the thruster fails to operate below 550 V dc ($E = CV^2/2$). The impulse bit and the energy relationship of the LES-6 thruster are expressed in Eq. (4):

$$I_b = 15.58\ E - 2.20\ \mu N\text{-}s \tag{4}$$

where I_b is the impulse bit in μN-s (μlb-s), E is the input energy in joules, and the numerical constants are dependent on the frontal area of the bar and the igniter resistance and include a unit conversion factor. The impulse bit repeatability at a constant input energy, constant frontal area of the Teflon bar, and constant igniter resistance is discussed in Section V. The 0.25-joule energy point is the interception of the energy axis by the extension of the impulse bit curve.

C.   Input Energy of the Main Discharge Capacitor and the
     Time Average Thrust

From the available test data taken at various pulse rates and various
input voltages, the time average thrust was calculated and plotted against
the input energy of the main discharge capacitor (Fig. 7). It can be noted
from this figure that the time average thrust is directly proportional to the
pulse rate, the square of the input voltage, and the frontal area of the
teflon bar:

$$F = 5.171 \times 10^{-6} \times f \times S \times V^2 - 0.428 \quad \text{(micronewtons)} \qquad (5)$$

In Eq. (5), V is the applied voltage of the main discharge capacitor in V dc,
f is the frequency or the pulse rate in pulses/s, S is the frontal area of the
Teflon bar in square centimeters (square inches) and F is the output thrust
in micronewtons (micropounds). The numerical constants of Eq. (5) are
related to the value of the igniter resistance and include the conversion
factors. From both Eq. (5) and Fig. 7, it is obvious that with a given con-
stant frontal area of the Teflon bar and constant input voltage, the time
average thrust will be directly proportional to the ignition command rate.
Also, for a constant pulse rate and frontal area, the time average thrust will
be directly proportional to the square of the applied voltage or the input
energy of the main discharge capacitor. Furthermore, with the known pulse
rate, applied voltage, and output thrust, the approximate frontal area of the
Teflon bar can be calculated from Eq. (5). Hence at any desired pulse rate
(0.5 to 3.0 pulse/s), operative voltage (600 - 1550 V dc) and known area of
the Teflon bar, the time average thrust can be calculated by Eq. (5) or
estimated from Fig. 7. Figure 7 illustrates that all the time average thrust
curves have different positive slopes. The variation in slopes of the time
average curves are inherent in the general characteristics of the LES-6
thruster. Thus Figs. 6 and 7, along with Eq. (5), have outlined some basic
and general characteristics of the LES-6 thruster. These data are further
substantiated by specific data in Sections IV and V, used for determination
of the optimal conditions and method of operating the LES-6 thruster.

D.   Time Average Thrust vs Ignition Command Rate

From the master data table, the time average thrust vs ignition com-
mand rates were plotted as in Fig. 8. The curves in Fig. 8 represent the
straight lines through the corresponding data points. Since the master data

table was obtained at a fixed pulse rate and variable input voltages, some of the data points are noncoincidental with their curves. These deviations, for the most part, resulted from the continuous incremental changes of the frontal area of the Teflon bar at various pulse rates. The foregoing statement is further substantiated by Eq. (5), where the output time average thrust is directly proportional to the frontal area of the Teflon bar. Within the first 300,000 accumulative input pulses, the maximum variation of the frontal area of the Teflon bar and, correspondingly, the output thrust from Eq. (5) are estimated to be 12% of their maximum value. The maximum deviation between a data point and its curve of Fig. 8 is 11%, which itself is well within the estimated limit. In the analysis above, the input voltage and the pulse rate were assumed to be kept constant.

The foregoing discussion is further substantiated in Fig. 9, where the output thrust was measured with a known frontal area of the Teflon bar, known igniter resistance, and constant input voltage. The maximum deviation between the curve of Fig. 9 and the corresponding data point at unknown conditions is 15.7%. Approximately 12% of the deviation above resulted from the continuous variation of the frontal area of the Teflon bar. The remainder is believed to be due both to igniter resistance variation and to the low voltage operation. Thus, if the thruster is operated at two opposite and extreme conditions, the maximum output thrust and the impulse bit variations should not exceed 15.7% of their respective values. Table 2 represents the time average thrust values with constant frontal area of the Teflon bar, constant input energy, and constant igniter resistance.

E.   Time Average Thrust, Impulse Bit, and Active Area of Igniter

Time average thrust values were obtained from a thruster with a non-insulated igniter and were recorded as in Table 3. The corresponding time average thrust curves and the average impulse bit curve are shown in Figs. 10 and 11. Even with noninsulated igniters, both time average thrust and the average impulse bit are directly proportional to the input energy (Figs. 10 and 11). Direct comparison of the time average thrust curves of Figs. 7 and 10 indicate that the thruster without insulation (or larger active area) produced more thrust than the one with proper insulation (smaller active area). However, the increase in both time average thrust values and impulse bit were observed only above 1 joule of the input energy level. Below 1 joule

of the input energy level, both time average thrust and the impulse bit curves of the thruster with a noninsulated igniter were divergent from the corresponding curves of the thruster with a properly insulated igniter. From Fig. 11, it can be noted that with the larger active area of the igniter, the impulse bit was increased approximately 20% at 2.5 joules of input energy level.

Figure 12 is the front view of the propellant and igniter assembly of the LES-6 thruster, and Figs. 13 and 14 are the individual closeup views of the active areas of two igniters. Figures 12, 13, and 14 illustrate the difference in the geometry of two active areas and their effects on the ablated Teflon mass, the nature of depolymerization, and the amount and thickness of carbon deposits on both igniters. Due to improper ignition and incomplete depolymerization of the Teflon bar, a heavy film of carbon deposits was accumulated on the noninsulated igniter, causing preignition of the thruster. The experiment indicated that with a more nearly optimum geometry of the igniter and location of the igniter in relation to the Teflon bar, the output thrust and efficiency of the thruster can be improved. Figure 13 shows the designed active area of the igniter as semicircular. This configuration of the igniter active area causes the rectangular-faced propellant bar to become contoured during continuous operation. A change in frontal area as contouring takes place causes the characteristics time average thrust to vary with propellant area, as discussed. The observation above can be noted from Figs. 15, 16, and 17. Both Figs. 16 and 17 are photographs of the Teflon bars which were ignited and contoured with a properly insulated igniter, while Fig. 15 is a photograph of the Teflon bar which was ignited with a noninsulated igniter. All three photographs illustrate that each igniter had contoured the Teflon bar frontal area in accordance with its own area and geometry. In comparing Figs. 15 and 16, even though the active area of the igniter was increased (Fig. 15) and produced more output thrust, the incomplete depolymerization of the Teflon bar resulted in a less efficient system than if the same igniter active area has been properly designed into the system.

The nonignited segment $\boxed{\text{-A-}}$ of the Teflon bar within Fig. 16 is believed to have resulted from the misalignment of the center lines of both the igniter and the Teflon bar. Since the centerline of the igniter's active

area was nonsymmetrical and misaligned with the centerline of the Teflon bar, the corresponding discharge current density was nonuniform over the frontal area of the Teflon bar. Because of the above-described nonuniformity of the discharge current density, the resultant contoured area of the Teflon bar is a semi-S shape rather than an expected semicylindrical contoured area. The misalignment of the centerlines was somewhat corrected before initiating thrust measurement with a newly faced Teflon bar. The correction resulted in a smaller nonignited portion of the propellant, which can be observed in Fig. 17, where the newly faced bar accumulated 150,000 ignitions.

It should be noted that the experimental results discussed in this report were based on tests performed in an oil-diffusion-pumped vacuum system which is known to contribute to a carbonaceous buildup of deposits and burned propellant at the edges of the Teflon fuel bar. Tests performed on a LES-6 thruster at the Goddard Space Flight Center (Ref. 3) in an ion-pumped vacuum system resulted in the propellant being consumed relatively cleanly.

V. SPECIFIC CHARACTERISTICS OF THE LES-6 THRUSTER

In Section IV of this report, some of the general characteristics of the microthruster, along with some experimental data, were presented. Both output thrust and impulse bit were directly proportional to the active area of the igniter, frontal area of the Teflon bar, and input energy of the main discharge capacitor. The above characteristics and their parametric relationships were presented in Eqs. (4) and (5).

Some of the specific parameters of the thruster will be discussed in this section. Such parameters and characteristics are specific impulse, efficiency, specific thrust, propellant mass ablated per discharge, variation of the igniter resistance, impulse bit repeatability, and variation of the frontal area of the Teflon with respect to accumulative input pulses.

A.   Time Average Thrust and Impulse Bit Repeatability

In Section IV of this report, it was stated that the output thrust and the impulse bit were experiencing continuous changes as the number of accumulative ignitions were increased. These changes during the early cycle life of a thruster with a newly faced propellant rod are effected mostly by the change

in frontal area during the first few one hundred thousand cycles of "burn in" (Ref. 3). To investigate the repeatability of the output thrust and the impulse bit, an experiment with constant frontal area of the Teflon bar, constant input energy, and constant igniter resistance was initiated. The experiment was repeated several times and the results are presented in Table 4 and Fig. 18. From the data in Table 4, it can be noted that as long as the igniter resistance, area of Teflon bar, and input energy are kept constant, both the impulse bit and the output thrust will be repeatable within 2 to 3% of its value. The above experiments were initiated at 600×10^{-6} N/m^2 (4.5×10^{-6} torr) and at 25°C (77°F). The maximum time average thrust and the impulse bit range (maximum-minimum) were 1.33 μN (0.3 μlb) and 1.33 μN-s (0.3 μlb-s), respectively. A minimum 2 h vacuum stabilization period was granted between two consecutive thrust runs.

B. Impulse Bit and Ignition Command Rate

The following experiment was initiated to determine whether there was any variation in the impulse bit at various ignition command rates. The time average thrust at 1500 V dc input voltage and at various pulse rates was measured as in Table 5. The corresponding impulse bits were calculated and plotted as in Fig. 19. Irrespective of the ignition command rate, the impulse bit stays constant at a constant input energy level (Fig. 19). To produce a constant impulse bit at a given energy level, the frontal area of the bar and the igniter resistance must be kept constant. Some slight impulse bit deviations were observed at the operating pulse rates. The deviation is more pronounced between the highest and the lowest pulse rates (3.82 μN-s or 0.86 μlb-s). These deviations are believed to have resulted from temperature rise variations of the main discharge capacitor at various pulse rates. The foregoing experiment proved that the main discharge capacitor had a time constant large enough to charge to its maximum available voltage, that impulse bit at a given energy level is independent of the ignition command rate, and that time average thrust at a given energy level is directly proportional to the pulse rate.

C. Specific Impulse and Efficiency

After a newly faced Teflon bar was ignited for 95,000 accumulative ignitions, the frontal area and its weight were measured and recorded. The carbon deposits were removed from both the active area and the air gap of

the igniter so that its open circuit resistance measurement was 500 ohms.
The time average thrust measurement was completed at 1500 V dc and
1 pulse/s for 54,499 accumulative ignitions. Again the weight and the frontal
area of the Teflon bar, along with the igniter resistance, were measured and
recorded. This experiment contributed the necessary information for com-
puting the following specific parameters.

The approximate mass ablated per discharge was computed to be
11.6 μg discharge (0.409 μlb/discharge).

During the entire experiment, the frontal of the Teflon bar had experi-
enced an increase of 0.38 cm^2 (0.0589 in.^{2}). The average impulse bit was
33.58 μN-s (7.55 μlbs-s) and specific impulse of the thruster can be calcu-
lated by

$$I_{sp} + I_b / W_{pd} \qquad (6)$$

where I_b is the impulse bit in μN-s (μlb-s), W_{pd} is the mass ablated per
pulse in μg (μlb) and I_{sp} is the specific impulse in seconds. The specific
impulse for the above experiment was 298 s.

From the available data, the efficiency was calculated by

$$\eta = 1/2 \; \frac{I_b \times I_{sp}}{E} \, g \qquad (7)$$

as 2.2%, where η is the efficiency in percent, E is the input energy of the
main discharge capacitor in W-s, and g is the gravity in cm/s^2 (in./s^2).

The accumulative input energy of the above experiment was 105,817
joules, while the accumulative output thrust was 2,155,808 μN (484,669 μlb).
The thruster parametric data (Table 6) was prepared from the results of the
above experiment.

D.   Frontal Area of the Teflon Bar and the Accumulative Input Pulses

It was discussed in the previous sections that as the accumulative
ignitions of a newly faced Teflon bar were increased, the frontal area of the
bar experienced an increase. The statement above was based on the avail-
able area measurements at various accumulative input pulses. Such data

is plotted in Fig. 20 and can be verified with the actual photographs of the frontal areas at 330,000 and 150,000 accumulative input pulses as in Figs. 16 and 17.

As stated earlier, both time average thrust and the impulse bit are directly proportional to the frontal area of the Teflon bar. Since both specific impulse and efficiency are functions of impulse bit, it can be concluded that both parameters (I_{sp}, η) are also area-dependent.

E.   Continuous Pulsing and the Output Thrust

A thruster with a newly faced Teflon bar was ignited at 1 pulse/s and 1450 V dc of the main discharge capacitor. The pulsing of the thruster was continuous for a period of 8 h a day. The objective of the experiment was to prepare a graphical relationship between the time average thrust and the accumulative input pulses. Since the output thrust was measured at the end of each accumulative 1000 pulses, some fluctuations were observed in the output thrust. Conversely, at the end of each 8-h test period, the magnitude of the output thrust decreased by 25% of its daily initial value. Since the output thrust was not recorded continuously, the original objective of the experiment was not established. However, during the above experiment, several unknown characteristics of the thruster were discovered. One of the important observations was the backstreaming of the exhaust from the thruster. In Section IV of this report the size of the vacuum bell jar system and the approximate location of the thruster nozzle to the bell jar were outlined. It is believed that both the charged and the ionized particles, after being accelerated electromagnetically and gasdynamically by the thruster, collided with the bell jar surface and reflected back toward the thruster, thus creating the backstreaming condition. Because of the presence of the backstreaming condition and inadequate diffusion pump capacity, the contamination level within the vacuum system bell jar had stabilized and caused the vacuum level to reach approximately one decade lower vacuum level than the initial vacuum level. The condition above was also verified by observing the effect of high-level contamination on the damping fluid of the pendulum system. During the experiment, a thin film of contamination substance deposited on the damping fluid. After a few days of operation, the viscosity of the fluid was changed, and replacement with noncontaminated damping fluid became necessary. Also, due to the backstreaming condition, a heavier film of

carbon material was deposited on the igniter surface and caused the early misfiring of the thruster. The segment of the inner surface of the vacuum system bell jar across from the thruster nozzle had also accumulated a heavy film of black material. Chemical analysis of the deposited material on the bell jar surface indicated the material was mainly-composed of carbon atoms.

Time average thrust values of the newly faced Teflon bar are plotted against the accumulative input pulses as in Fig. 21.

F.   Intermittency of the Thruster

During the test and evaluation of the microthruster, its intermittency was observed on several occasions. The causes of the temporary malfunction of the thruster were investigated and have been outlined herein. Since it was believed that the misfiring or the intermittency of the thruster was caused by a variation of any one of several input parameters or components within the thruster itself, each item of concern will be discussed individually and their contribution(s) to the intermittency condition outlined accordingly.

1.   Input power requirement. The thruster requires a minimum of 600 V dc at the main discharge capacitor to operate properly. At any voltage less than 600 V dc, the thruster misfires and the percentage of misfiring increases as the input voltage decreases. The minimum input voltage requirement (600 V dc) was applicable only at lower pulse rates (0. 5 to 2. 0 pulses/s). At higher pulse rates (2. 5 to 3. 0 pulses/s) the thruster started misfiring at high voltages (800 to 1200 V dc) and as the ignition command rate was increased, the misfiring percentage increased. The misfiring at higher pulse rates and at higher input voltage levels was believed to result both from an accelerated temperature rise of the main discharge capacitor at higher pulse rates and from the limitations imposed by the electronics components within the thruster.

2.   Igniter resistance and its variation. Previous sections stated that carbon deposits resulting from accumulative ignitions of the Teflon bar were observed on the surface of the igniter plug. The carbon deposits on the igniter plug and its air gap acted as a parallel resistance with the igniter circuit and thus caused a large range variation in the igniter resistance. Such variation in the resistance was measured from 0. 5 to 1500 ohms. The misfiring with low igniter resistance was interpreted to be due to the

lower time constant (τ = RC) that the igniter capacitor would have in such a condition. Since the igniter capacitor's time constant was not large enough, the capacitor was unable to charge to its maximum value of the available voltage, and thus intermittency resulted. This observation could have been substantiated by adding series or parallel resistances to the igniter circuit and then observing the effects on both the performance and the intermittency of the thruster.

The early misfiring resulted from operating the thruster in either a low main discharge voltage (1100 V dc and lower) or operating the thruster continuously for an 8-h period every day. Both operational modes caused heavy carbon material deposits on the igniter surface and thus resulted in lower igniter resistance. At lower operating voltages, the insufficient energy of the main discharge capacitor was unable to produce a complete polymerization condition as in the higher-voltage operation. This incomplete depolymerization of the Teflon bar created an excess amount of carbon, which was deposited on the igniter surface and caused the observed intermittency. The discussion of the effect of continuous pulsing (Subsection E above) noted that due to the limitation in the diffusion pump capacity of the vacuum system, part of the exhausted carbon material was returned into the thruster and deposited on the igniter surface.

3.   Active area of the igniter and its geometry. The proper geometry of the igniter active area and its relative alignment with the propellant bar was another contributing factor for the misfiring of the thruster. Due to the misalignment between the centerlines of the igniter and the propellant bar, the bar was contoured more at one edge than on the opposite edge. Thus, due to the nonsymmetric ignitions, the corner of the bar furthest from the igniter centerline was not polymerized completely and had extended and covered a segment of the igniter's active area. This small active area of the igniter, along with carbon deposits on it, caused the thruster to misfire after 300,000 accumulative ignitions.

4.   Electrical insulation. In the previous sections of this report, some of the arcing problems were presented, and it was stated that such problems were eliminated. During several experiments, due to arcing, the main discharge capacitor did not receive sufficient input energy and thus failed to deliver the required energy for the polymerization process. The

arcing problems were eliminated by installing proper insulation within the system, eliminating the previously observed intermittency. Even though arcing is not a design characteristic of the thruster, it requires special attention in the application of the thruster within any system. The experiments made their contributions by outlining that one of the possible contributing sources of the intermittency could be the poor electrical insulation of any thruster system in a vacuum environment.

5. <u>Energy level of the igniter capacitor</u>. The igniter capacitor was charged from 227 V dc up to 597 V dc and at present the minimum voltage required for normal operation has not been determined. GSFC has initiated some experiments and has discovered that the thruster misfired at 90 V dc of the ignition discharge voltage. The misfiring percentage decreased as the ignition voltage increased toward 115 V dc. The thruster was operated without misfiring at the ignition voltage of 115 V dc. Since the upper limits of the igniter voltage are determined by the silicon-controlled rectifier within the igniter circuit (600 V dc), the igniter voltage range of the LES thruster for normal operation can be set from 115 to 600 V dc.

VI. COMPARATIVE TEST DATA

The objective of this section is to outline, compare, and establish any correlation among those data obtained by GSFC, MIT Lincoln Laboratory and JPL. Although both MIT (Refs. 4 and 5) and GSFC have been evaluating and investigating the LES-6 thruster and its characteristics for longer periods than JPL has, the data obtained by JPL has correlated with those obtained by the above institutions. The average impulse bits vs the input energy of the main discharge capacitor obtained by the three institutions are shown in Fig. 22. As can be seen from Fig. 22, those data points obtained by both JPL and GSFC are less scattered than those obtained by MIT. In general, the data obtained by the three institutions indicates that impulse bit is directly proportional to the input energy of the main discharge capacitor. If a straight line is drawn through each set of data points, the extension of these lines will intercept the energy axis at approximately 0.25 to 0.30 joules. The energy axis interception points clearly indicate that the thruster will require a minimum of 500 to 600 V dc as the main discharge voltage to initiate firing.

Strong correlations between JPL and GSFC data are mainly the slopes of the impulse bit curves and the energy axis interception points. However, some slight deviations in impulse bit measurements can be observed and are believed to have resulted from the difference between the frontal areas of the Teflon bars. GSFC data correspond to approximately 2.89 cm^2 (0.4479 $in.^2$) of the frontal area of the Teflon bar, and JPL readings correspond to 3.08 cm^2 (0.4774 $in.^2$) of the same area at 150,000 accumulative ignitions. Since the measurements of the frontal area of the Teflon bar by MIT were not available, a similar comparison of these data was not made. Thus, the reasons for lower impulse bit values obtained by MIT are yet to be determined. A parametric table of data from the three institutions is presented in Table 7.

It can be seen from Table 7 that the general trend of data in each of the columns is in agreement. However, there are some discrepancies such as those in the igniter resistances, approximate Teflon bar areas, and impulse bit repeatabilities. The variation in impulse bit repeatabilities is caused by the difference between the frontal areas of the Teflon bars under ignition.

Other minor deviations among the parameters may be contributed by different thrusters and their manufacturing tolerances. The difference in the test setups and methods of calibration by each institution can also be a contributing factor to minor deviations.

VII. CONCLUSION AND SUMMARY

Preliminary information about the LES-6 thruster has been acquired with the aid of the torsion pendulum system. The information consisted of the general characteristics of the LES-6 thruster which established and verified some mathematical relationships between the input and the output parameters. The parameters of interest, such as time average thrust, impulse bit, efficiency and specific impulse, were studied under various input conditions. The test data indicate that the LES-6 thruster, with some identifiable design improvements, represents an attractive reaction control thruster for attitude control applications on long-life spacecraft requiring small, metered impulse bits for precise pointing control of science instruments.

Prior to further application of a LES-6-type pulsed plasma thruster, the following studies and evaluations are required. The effect of temperature on the thruster's performance is needed. Both the upper and lower temperature limitations must be understood. The content and the composition of the accelerated particles and possible backstreaming characteristics by the thruster need to be investigated.

Since both the time average thrust and the impulse bit are area-dependent, it is suggested that prior to any flight operation, solid propellant pulsed plasma thrusters be discharged at least 200,000 times. The minimum main discharge operative voltage is recommended to be greater than 1400 V dc for sustained firing.

The igniter plug and its circuit elements are known to influence the output thrust and the impulse bit significantly. The continuous variation of the igniter resistance due to the accumulative carbon deposits indicates that the igniter circuit and the igniter's physical configuration require further modification on the basis of the results presented. However, GSFC investigations have revealed that by increasing the nominal main capacitor voltage from 1360 V, as used on the MIT Lincoln Laboratory satellite, to 1450 V, the deposit buildup is greatly reduced. The deposit accumulation on the igniter correspondingly appeared to be far less than observed in the JPL experiments. The igniter resistance during endurance testing at GSFC dropped to a value of 90 ohms over 2,000,000 cycles. As has been pointed out, the igniter assembly can no doubt be improved to extend the life capability for the LES-6 engine; however, the present design appears to offer a thruster with a cycle life well in excess of 1,000,000 cycles under specified operating conditions.

REFERENCES

1. Guman, W., _Pulsed Plasma Technology in Microthrusters_, Technical Report AFAPL-TR-68-132, Fairchild Hiller Corporation, Republic Aviation Division, November 1968.

2. Malherbe, P., Vogt, T., and Boebel, C., "Impulse Measurements of Electrical Engines by a Vacuum Microbalance Technique," _Vacuum Microbalance Techniques_, Vol. V, Plenum Press, New York, 1966.

3. Williams, T., and Callens, R., "Performance Testing of a Solid Propellant Pulsed Plasma Microthruster," NASA Goddard Space Flight Center, AIAA Paper 72-460, presented at the AIAA 9th Electric Propulsion Conference, April 1972.

4. Vondra, R. J., and Solbes, A., "Performance Study of a Solid Fuel Pulsed Electric Microthruster," Massachusetts Institute of Technology Lincoln Laboratory, AIAA Paper 72-458, presented at the AIAA 9th Electric Propulsion Conference, April 1972.

5. Vondra, R. J., _Performance Optimization of a Solid Fuel Microthruster_, Report No. 1, Massachusetts Institute of Technology Space Propulsion Laboratory, January 1971.

Table 1. Master thrust data table

Average thrust F, μN (μlb), and impulse bit I_b, μN-s (μlb-s), for indicated ignition command rate in pulses/second (pps)

Main Discharge Voltage (vdc)	Ignition Voltage (vdc)	0.50 pps F	0.50 pps I_b	0.75 pps F	0.75 pps I_b	1.00 pps F	1.00 pps I_b	1.25 pps F	1.25 pps I_b	1.50 pps F	1.50 pps I_b	1.75 pps F	1.75 pps I_b	2.00 pps F	2.00 pps I_b	2.25 pps F	2.25 pps I_b	2.50 pps F	2.50 pps I_b	2.75 pps F	2.75 pps I_b	3.00 pps F	3.00 pps I_b
1550	597	19.04 (4.28)	38.07 (8.56)	27.0 (6.07)	36.03 (8.1)	---	---	49.15 (11.05)	39.14 (8.8)	---	---	67.17 (15.1)	38.34 (8.62)	72.06 (16.2)	36.03 (8.1)	74.95 (16.85)	33.1 (7.5)	80.51 (18.1)	32.20 (7.23)	95.63 (21.5)	34.78 (7.85)	102.75 (23.1)	34.25 (7.7)
1500	577	17.88 (4.02)	35.76 (8.04)	25.93 (5.83)	34.65 (7.79)	35.36 (7.95)	35.36 (7.95)	42.97 (9.66)	34.25 (7.7)	59.6 (11.6)	34.47 (7.75)	61.38 (13.8)	35.14 (7.9)	66.41 (14.93)	33.20 (7.47)	70.28 (15.8)	31.24 (7.05)	74.73 (16.8)	29.89 (6.77)	90.74 (20.4)	33.0 (7.44)	95.19 (21.4)	31.73 (7.18)
1450	558	16.59 (3.73)	33.18 (7.46)	24.86 (5.59)	33.14 (7.45)	33.14 (7.45)	33.14 (7.45)	40.12 (9.02)	32.03 (7.2)	48.92 (11.0)	32.65 (7.34)	57.16 (12.85)	32.65 (7.34)	61.38 (13.8)	30.69 (6.9)	65.39 (14.7)	29.06 (6.55)	71.17 (16.0)	28.47 (6.45)	85.85 (19.3)	31.22 (7.03)	92.07 (20.7)	30.69 (6.92)
1400	540	15.35 (3.45)	30.69 (6.9)	23.71 (5.33)	31.58 (7.1)	30.71 (6.91)	30.71 (6.91)	36.79 (8.27)	29.36 (6.6)	46.26 (10.4)	30.83 (6.93)	52.93 (11.9)	30.25 (6.8)	55.69 (12.52)	27.85 (6.26)	61.38 (13.8)	27.28 (6.15)	67.61 (15.2)	27.04 (6.15)	81.84 (18.4)	29.76 (6.7)	83.85 (18.85)	27.95 (6.76)
1350	520	14.23 (3.20)	28.47 (6.40)	21.48 (4.83)	28.70 (6.45)	28.8 (6.48)	28.8 (6.48)	33.45 (7.52)	26.69 (6.0)	42.61 (9.58)	28.39 (6.38)	48.48 (10.9)	27.71 (6.23)	51.15 (11.5)	25.58 (5.75)	59.16 (13.3)	26.29 (5.92)	63.16 (14.2)	25.26 (5.7)	75.62 (17.0)	27.50 (6.18)	77.84 (17.5)	25.95 (5.82)
1300	502	12.05 (2.71)	24.11 (5.42)	19.44 (4.37)	25.89 (5.82)	26.11 (5.87)	26.11 (5.87)	29.50 (6.63)	23.57 (5.3)	38.48 (8.65)	25.75 (5.79)	42.92 (9.65)	24.55 (5.52)	45.59 (10.25)	22.8 (5.13)	55.82 (12.55)	24.81 (5.57)	59.60 (13.4)	23.84 (5.37)	69.83 (15.7)	25.39 (5.72)	74.73 (16.8)	24.91 (5.61)
1250	482	10.90 (2.45)	21.8 (4.9)	16.55 (3.72)	22.06 (4.96)	23.71 (5.33)	23.71 (5.33)	27.27 (6.13)	21.8 (4.9)	36.07 (8.11)	24.02 (5.4)	39.5 (8.88)	22.55 (5.07)	40.7 (9.15)	20.35 (4.58)	47.59 (10.7)	21.15 (5.2)	56.05 (12.6)	22.42 (5.04)	64.5 (14.5)	23.45 (5.27)	68.94 (15.5)	22.98 (5.27)
1200	463	9.47 (2.13)	18.95 (4.26)	14.23 (3.20)	19.0 (4.27)	22.55 (5.07)	22.55 (5.07)	24.02 (5.4)	19.13 (4.3)	33.0 (7.42)	22.02 (4.95)	35.14 (7.9)	20.08 (4.51)	36.74 (8.26)	18.37 (4.13)	43.15 (9.7)	19.18 (4.32)	53.38 (12.0)	21.35 (4.8)	58.71 (13.2)	21.35 (4.81)	62.27 (14.0)	20.76 (4.67)
1150	444	8.36 (1.88)	16.73 (3.76)	13.26 (2.98)	17.66 (3.97)	20.81 (4.68)	20.81 (4.68)	21.8 (4.9)	17.35 (3.9)	29.58 (6.65)	19.71 (4.43)	32.38 (7.28)	18.50 (4.15)	32.3 (7.26)	16.15 (3.63)	38.48 (8.65)	17.1 (3.85)	47.59 (10.7)	19.03 (4.27)	54.27 (12.2)	19.74 (4.43)	⊖	⊖
1100	424	6.98 (1.57)	13.97 (3.14)	11.70 (2.63)	15.61 (3.51)	16.55 (3.72)	16.55 (3.72)	16.73 (3.76)	13.34 (3.0)	27.49 (6.18)	18.28 (4.11)	29.05 (6.53)	16.6 (3.7)	27.85 (6.26)	13.93 (3.13)	32.38 (7.28)	14.39 (3.28)	40.3 (9.06)	16.12 (3.62)	49.37 (11.1)	17.95 (4.02)		
1050	402	6.14 (1.38)	12.28 (2.76)	10.59 (2.38)	14.10 (3.17)	15.21 (3.42)	15.21 (3.42)	14.5 (3.26)	11.56 (2.6)	23.71 (5.33)	15.79 (3.55)	25.67 (5.77)	14.67 (3.28)	22.33 (5.02)	11.16 (2.51)	30.16 (6.78)	13.40 (3.03)	38.03 (8.55)	15.21 (3.42)	44.26 (9.95)	16.09 (3.5)		
1000	382	4.76 (1.07)	9.52 (2.14)	9.47 (2.13)	12.63 (2.84)	12.68 (2.85)	12.68 (2.85)	⊖	⊖	20.33 (4.57)	13.52 (3.04)	23.4 (5.26)	13.37 (3.0)	20.19 (4.54)	10.1 (2.27)	27.93 (6.28)	12.41 (2.8)	34.56 (7.77)	13.82 (3.11)	39.14 (8.8)	14.23 (3.2)		
950	366	⊖	⊖	8.1 (1.82)	10.81 (2.43)	10.85 (2.44)	10.85 (2.44)			16.59 (3.73)	10.85 (2.49)	20.11 (4.52)	11.49 (2.58)	19.48 (4.38)	9.74 (2.19)	23.8 (5.35)	10.58 (2.38)	31.40 (7.06)	12.56 (2.83)	⊖	⊖		
900	347			6.98 (1.57)	9.30 (2.09)	10.63 (2.39)	10.63 (2.39)			15.39 (3.46)	10.23 (2.3)	17.84 (4.01)	10.19 (2.29)	17.26 (3.88)	8.63 (1.99)	21.26 (4.78)	9.45 (2.12)	23.8 (5.35)	9.52 (2.14)				
850	326			⊖	⊖	8.27 (1.86)	8.27 (1.86)			12.99 (2.92)	8.63 (1.94)	15.61 (3.51)	8.92 (2.0)	15.03 (3.38)	7.52 (1.69)	17.93 (4.03)	7.97 (1.8)	21.35 (4.8)	8.58 (1.92)				
800	308					6.67 (1.5)	6.67 (1.5)			10.14 (2.28)	6.76 (1.52)	13.92 (3.13)	7.95 (1.79)	12.23 (2.75)	6.11 (1.38)	15.57 (3.5)	6.92 (1.55)	13.97 (3.14)	5.59 (1.26)				
750	288					⊖	⊖			⊖	⊖	11.17 (2.51)	6.38 (1.43)	10.1 (2.27)	5.05 (1.13)	10.59 (2.38)	4.71 (1.05)	⊖	⊖				
700	270											9.21 (2.07)	5.26 (1.18)	7.83 (1.76)	3.92 (0.88)	7.12 (1.6)	3.16 (0.72)						
650	250											6.94 (1.56)	3.97 (0.90)	⊖	⊖	⊖	⊖						
600	231											4.80 (1.08)	2.74 (0.62)	---	---	---	---						

⊖ – Thruster failed to respond to the ignition command signal.

Table 2. Time average thrust vs ignition command rate (input voltage 1500 V dc, ignition voltage 597 V dc, frontal area of the Teflon bar 3.0 cm^2 (.465 in.^{2}) and igniter resistance $\approx$ 500Ω)

Pulse Rate, pps	Time Average Thrust, μN (μlbs)	
3	97.86	(22)
2.75	89.18	(20.05)
2.50	85.18	(19.15)
2.25	76.06	(17.1)
2.0	67.61	(15.2)
1.75	59.38	(13.35)
1.50	52.26	(11.75)
1.25	43.59	(9.8)
1.00	33.67	(7.57)
0.75	27.22	(6.12)
0.50	18.42	(4.14)

Table 3. Time average thrust data from the thruster with noninsulated igniter

Pulse Rate pps	Parameter	Time average thrust F, μN (μlb), and impulse bit I_b, μN-s (μlb-s) for indicated input voltage, V dc, of the main discharge capacitor																	
		1550	1500	1450	1400	1350	1300	1250	1200	1150	1100	1050	1000	950	900	850	800	750	700
1	F	45.37 (10.2)	42.03 (9.45)	39.14 (8.8)	35.36 (7.95)	32.47 (7.3)	29.36 (6.6)	26.91 (6.05)	24.02 (5.4)	21.8 (4.9)	19.57 (4.4)	16.46 (3.7)	15.12 (3.4)	12.63 (2.84)	10.68 (2.4)	8.45 (1.9)	6.72 (1.51)	5.07 (1.14)	3.65 (0.82)
1	I_b	45.37 (10.2)	42.03 (9.45)	39.14 (8.8)	35.36 (7.95)	32.47 (7.3)	29.36 (6.6)	26.91 (6.05)	24.02 (5.4)	21.8 (4.9)	19.57 (4.4)	16.46 (3.7)	15.12 (3.4)	12.63 (2.84)	10.68 (2.4)	8.45 (1.9)	6.72 (1.51)	5.07 (1.14)	3.65 (0.82)
1.5	F	61.83 (13.9)	57.38 (12.9)	54.27 (12.2)	49.82 (11.2)	45.81 (10.3)	42.7 (9.6)	38.7 (8.7)	34.69 (7.8)	31.36 (7.05)	27.13 (6.1)	24.02 (5.4)	20.46 (4.6)	17.93 (4.03)	15.12 (3.4)	12.32 (2.77)	10.36 (2.33)	7.83 (1.76)	5.6 (1.26)
1.5	I_b	41.22 (9.25)	38.25 (8.6)	36.18 (8.13)	33.21 (7.45)	30.55 (6.9)	28.47 (6.9)	25.8 (5.5)	23.13 (5.2)	20.91 (4.7)	18.09 (4.08)	16.01 (3.6)	13.64 (3.06)	11.95 (2.7)	10.08 (2.26)	8.21 (1.85)	6.91 (1.55)	5.22 (1.17)	3.74 (0.84)

Table 4. Time average thrust and impulse bit repeatability test with constant frontal area of the Teflon bar and constant igniter resistance (3.26 cm^2 or 0.505 in.^{2} and 3.5 ohms). Tests were performed at 1500 V dc main discharge voltage, 597 V dc igniter voltage, and 1 pps of ignition command rate

Test No.	Time Average Thrust in Micronewtons (Micropounds)	Impulse Bit Micronewton-Second (Micropound-Second)
1	35.45 (7.97)	35.45 (7.97)
2	36.65 (8.24)	36.65 (8.24)
3	35.45 (7.97)	35.45 (7.97)
4	35.72 (8.03)	35.72 (8.03)
5	35.45 (7.97)	35.45 (7.97)
6	36.2 (8.14)	36.2 (8.14)
7	36.61 (8.23)	36.61 (8.23)
8	35.5 (7.98)	35.5 (7.98)
9	35.1 (7.89)	35.1 (7.89)
10	36.65 (8.24)	36.65 (8.24)
11	36.7 (8.25)	36.7 (8.25)
12	36.61 (8.23)	36.61 (8.23)

Table 5. Time average thrust and impulse bit data table at 2.25 joules, 500 ohms igniter resistance, and 2.986 cm^2 (0.463 in.^{2}) of Teflon bar frontal area

Pulse Rate pps	Time Average Thrust μN (μlb)	Impulse Bit μN-s (μlb-s)
3.0	97.86 (22.00)	32.62 (7.33)
2.75	89.18 (20.05)	32.43 (7.34)
2.50	85.18 (19.15)	34.07 (7.64)
2.25	76.06 (17.1)	33.80 (7.60)
2.0	67.61 (15.2)	33.80 (7.60)
1.75	59.38 (13.35)	33.93 (7.62)
1.50	52.26 (11.75)	34.84 (7.82)
1.25	43.59 (9.8)	33.36 (7.5)
1.0	33.36 (7.5)	33.36 (7.5)
0.75	27.22 (6.12)	36.29 (8.14)
0.50	18.41 (4.14)	36.82 (8.23)

Table 6. Parametric data table of the LES-6 thruster

Specific Impulse Seconds	Efficiency %	Mass Ablated Per Discharge μgrams/ Discharge (μlbs/ Discharge)	Energy Per Pulse joules/ Discharge	Specific Thrust μN/ joule (μlbs/ joule)	Specific Energy joules/ μN (joules/ μlb)	Energy Per Unit Area joules/cm^2 (joules/in^2)
298	2.2	11.6 (0.409)	1.945	17.35 (3.9)	0.058 (0.259)	0.597 (3.85)

Table 7. Parametric data obtained by GSFC, MIT, and JPL

Parameter Under Study	GSFC	MIT, Lincoln Lab	JPL
Specific Impulse Sec	264 Within first 150,000 accumulative ignitions	340	298 Within first 150,000 accumulative ignitions.
Efficiency%	2.12 within first 150,000 accumulative ignitions	2.21	2.2 within first 150,000 accumulative ignitions.
Mass Ablated per Discharge μgrams/pulse (μlbs/pulse)	13.65(0.48) averaged over 1.1×10^6 accumulative ignitions.	10-12.5 (0.353-0.44)	11.6(0.409) averaged from 95,000 to 150,000 accumlative ignitions.
Energy per Discharge joules/pulse	~2.0	--	1.945
Specific Thrust μN/Joule (μlbs/joule)	0.863(3.84)	0.674-0.899 ~(3 - 4)	0.877(3.9)
Specific Energy Joules/μN (joules/μlb)	0.063(0.28)	--	0.058(.259)
Energy per Unit Area Joules/cm^2 (joules/in^2)	0.656(4.23)	--	0.597(3.85)
Igniter Resistance Variation Ω	7 - 105	--	3.2 to 1500
Impulse Bit Repeatability %	10 - 11 Total	--	5 (with constant bar area and igniter resistance)
Approx. Bar Area After 150,000 Ignitions $cm^2(in^2)$	3.05(0.473)	--	3.26(0.505)
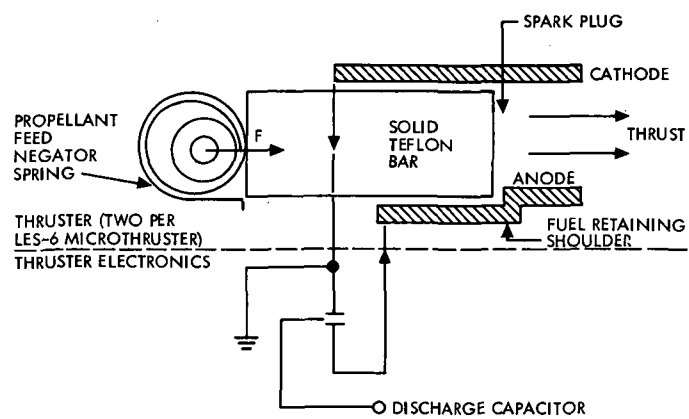
Fig. 1. Schematic diagram of the LES-6 microthruster
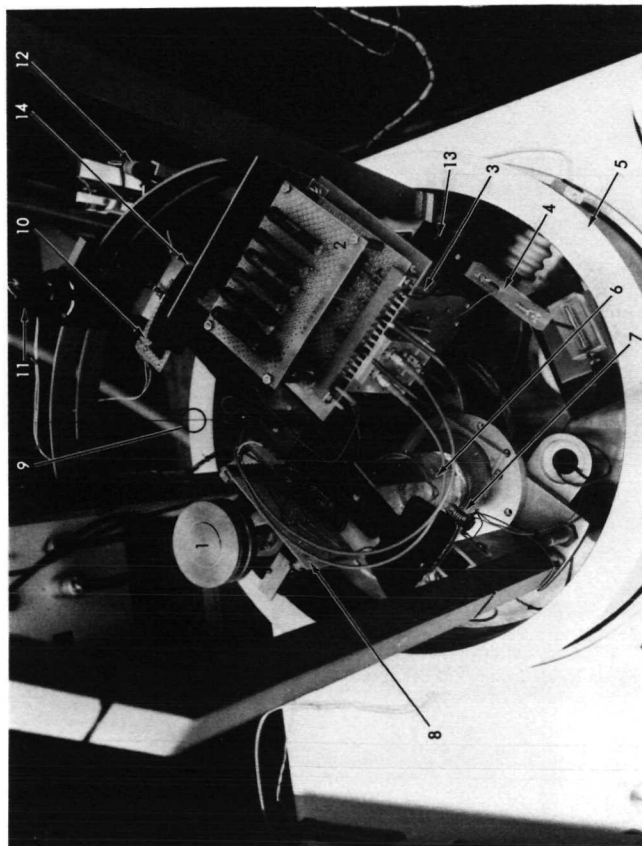
1 – COUNTER BALANCE WEIGHT
2 – VOLTAGE DIVIDING NETWORK
3 – LES-6 THRUSTER
4 – PIN & MERCURY POOL ASSY
     (MAIN DISCHARGE CAPACITOR)
5 – VACUUM BELL JAR RING
6 – DAMPING MECHANISM
7 – OPTICAL COMMAND SOURCE

8 – TRIGGER NETWORK
9 – TORSION WIRE
10 – READOUT PHOTOCELL BANK
11 – READOUT LIGHT SOURCE
12 – THRUSTER RESPONSE, PHOTOSENSOR
13 – PLATFORM
14 – SHADOW PLATE

Fig. 2. Torsion pendulum assembly
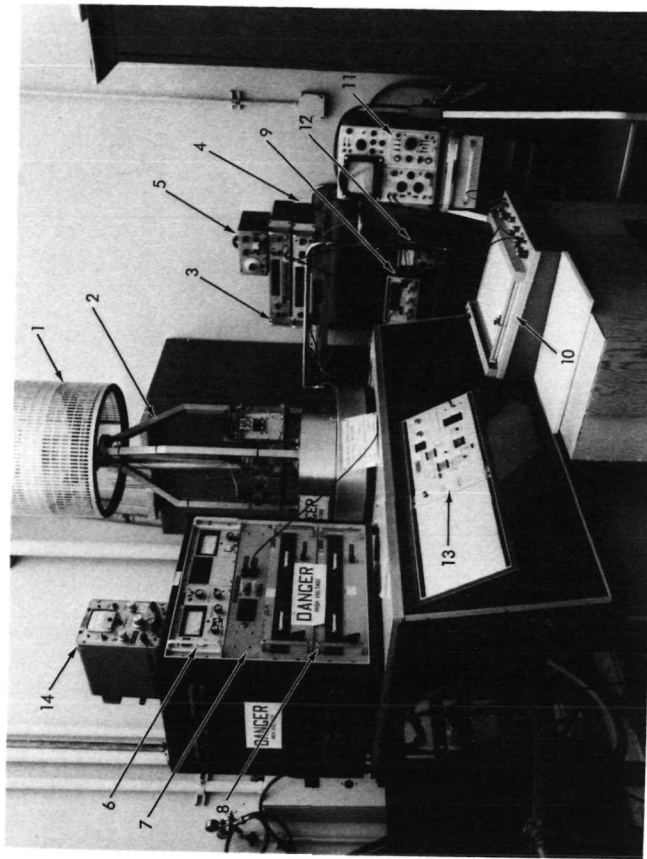
1 – BELL JAR VACUUM SYSTEM
2 – SUPPORTING STRUCTURE, TORSION
     PENDULUM
3 – DISPLAY OF IGNITION COMMAND RATE
4 – ACCUMULATIVE INPUT PULSES
5 – PULSE GENERATOR
6 – IONIZATION GAUGE
7 – THRUSTER RESPONSE. COUNTER

8 – MAIN POWER SUPPLY
9 – DIGITAL VOLT-METER
10 – X-Y PLOTTER
11 – OSCILLOSCOPE
12 – POWER SUPPLY OPTICAL COUPLER
13 – VACUUM SYSTEM CONTROL PANEL
14 – POWER SUPPLY, OUTPUT COUNTER

Fig. 3. Torsion pendulum and its instrumentation
system
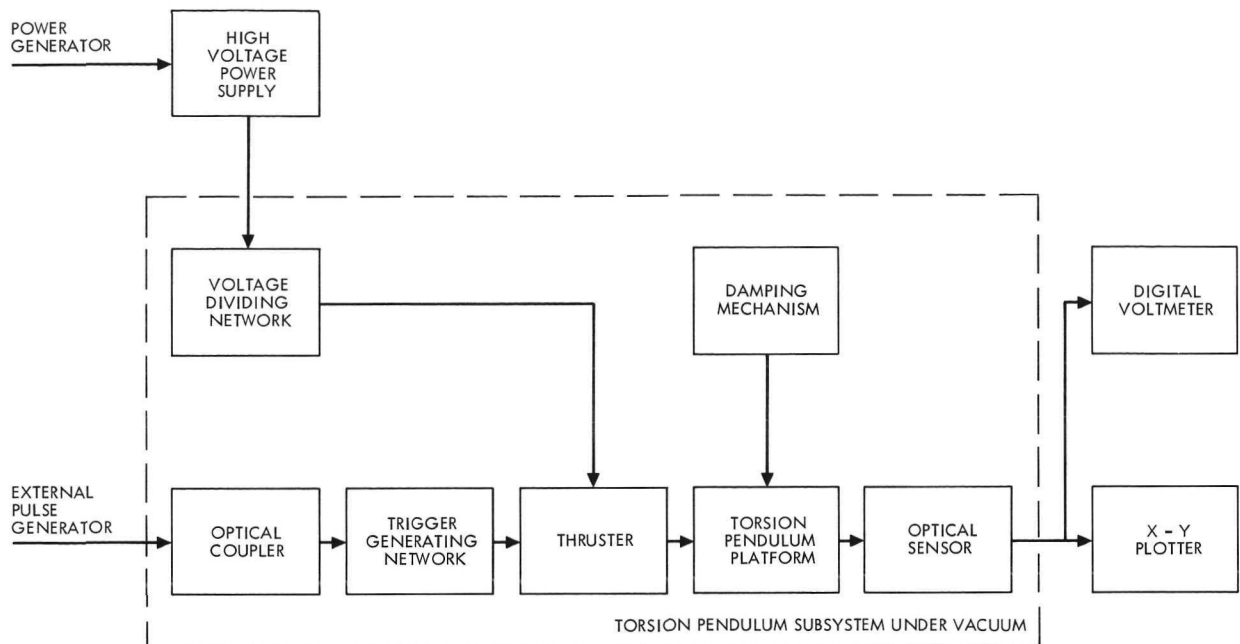
Fig. 4. Functional block diagram of torsion pendulum system
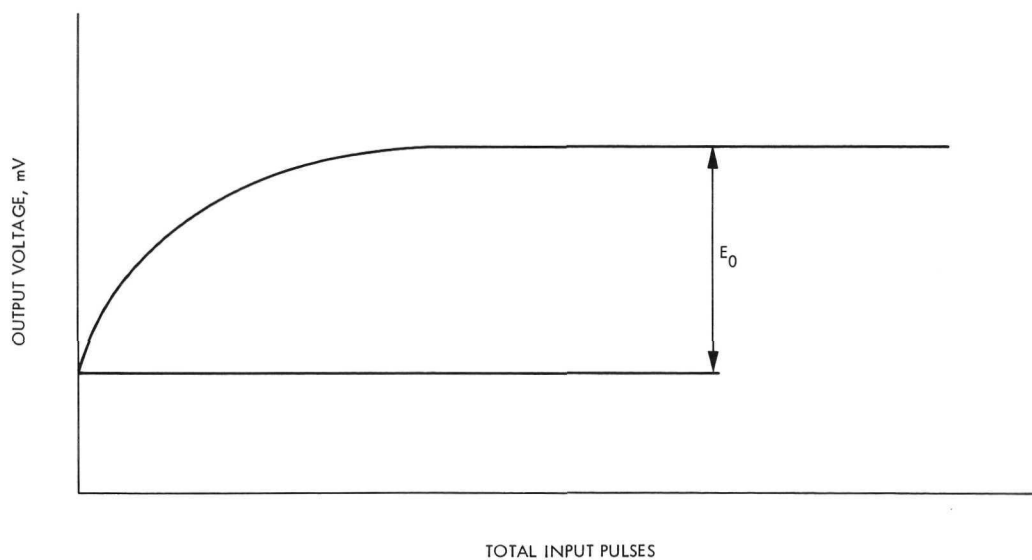
Fig. 5. Time average thrust response of the torsion pendulum
system to the output thrust of the LES-6 thruster
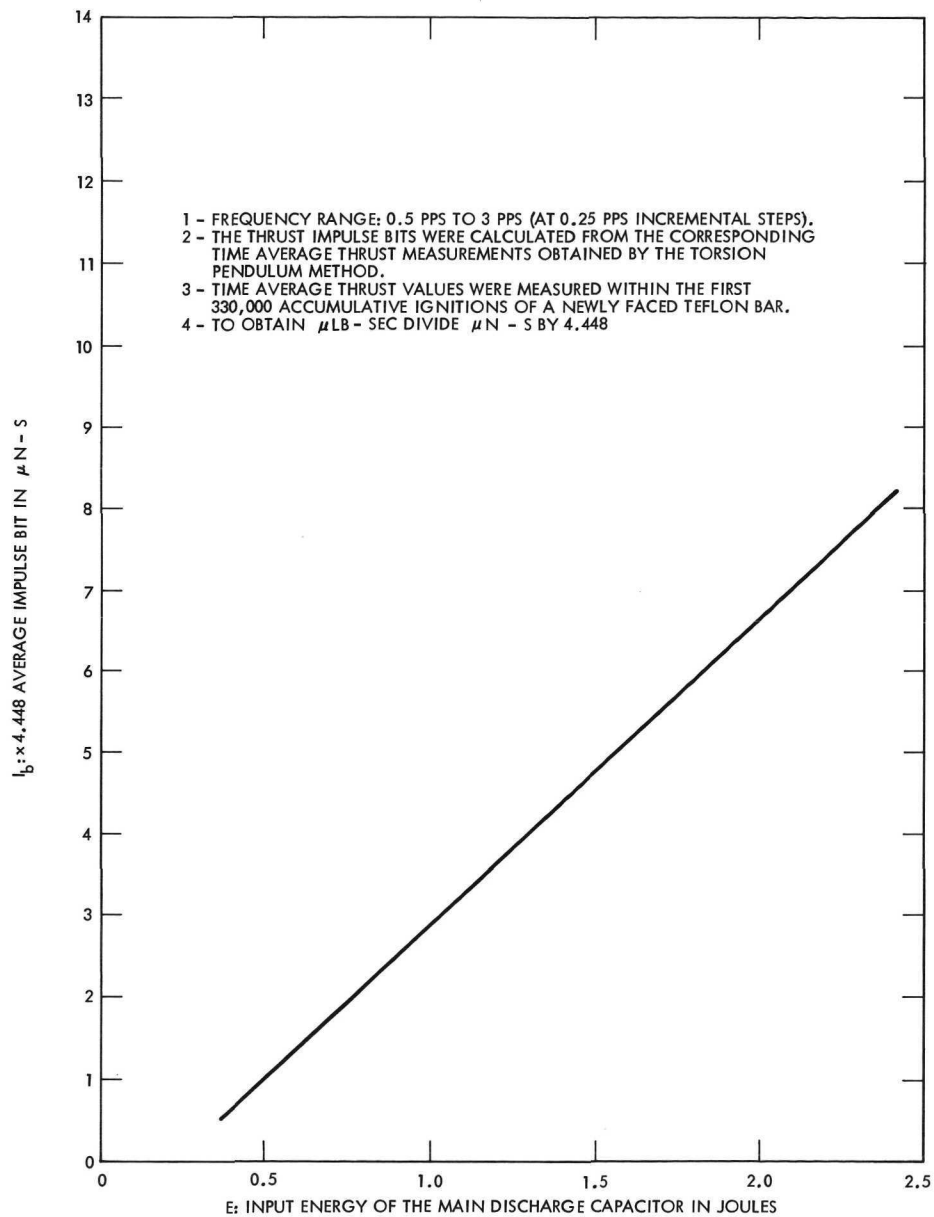
Fig. 6. Average impulse bit vs input energy
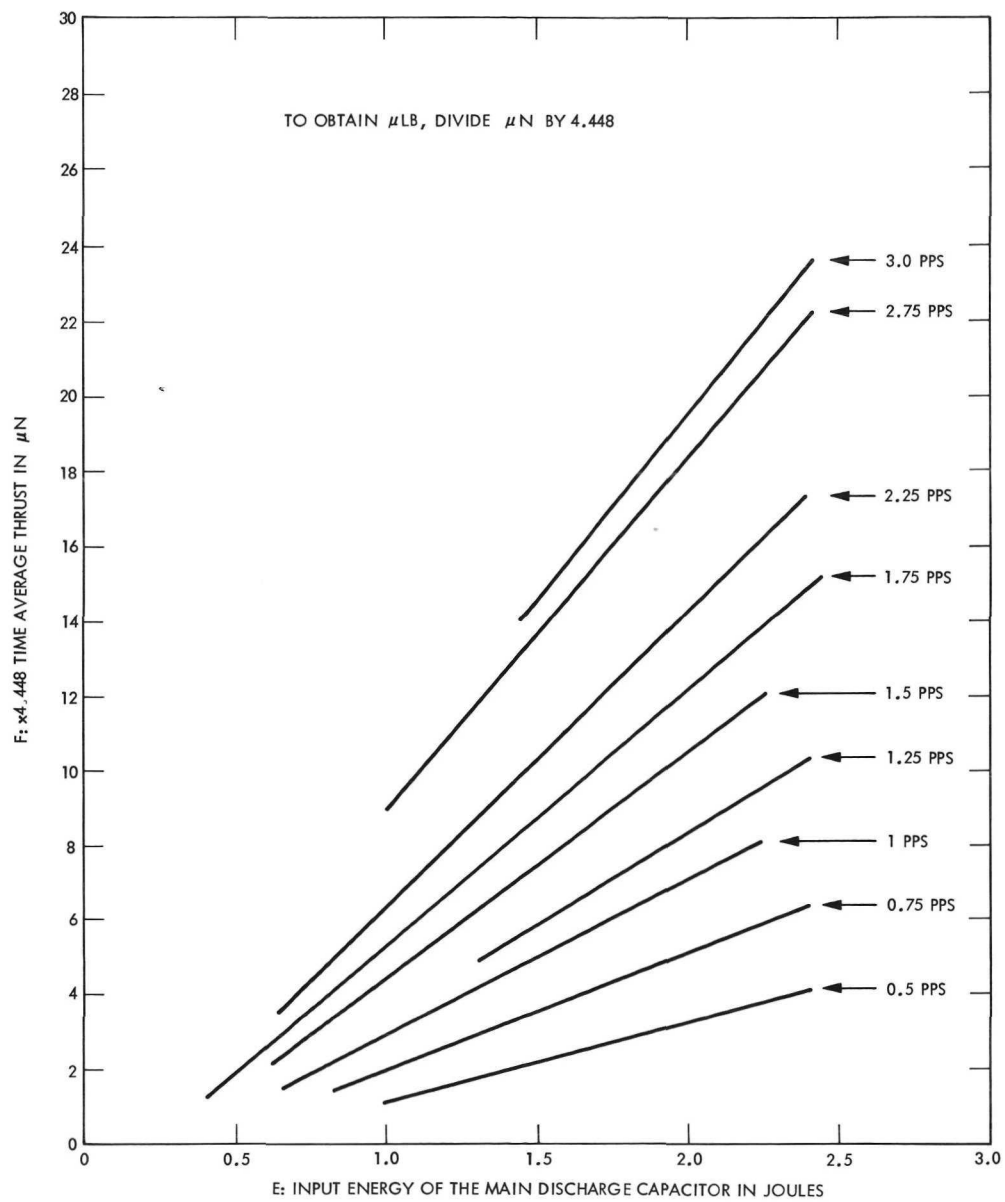
Fig. 7. Time average thrust vs input energy
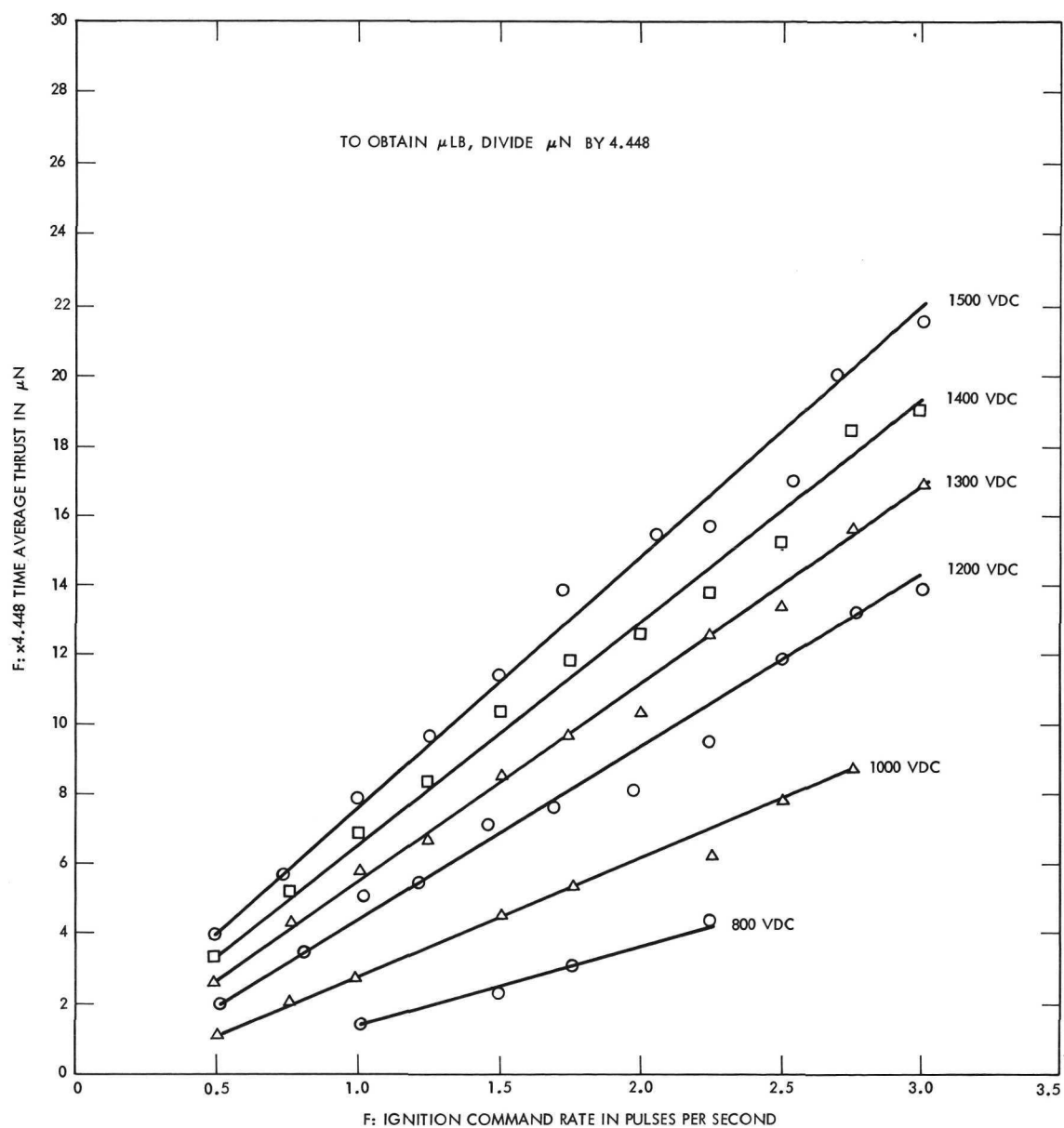
Fig. 8. Time average thrust vs ignition command rate
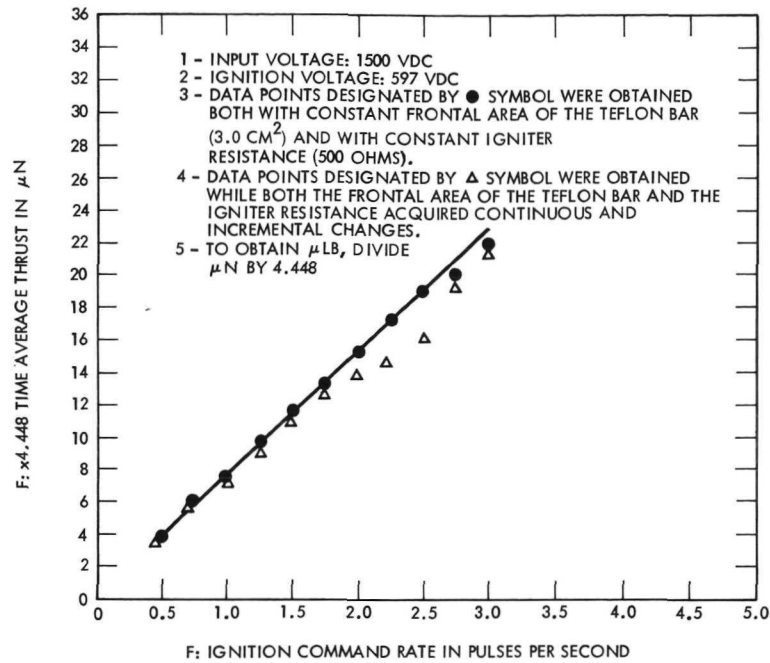
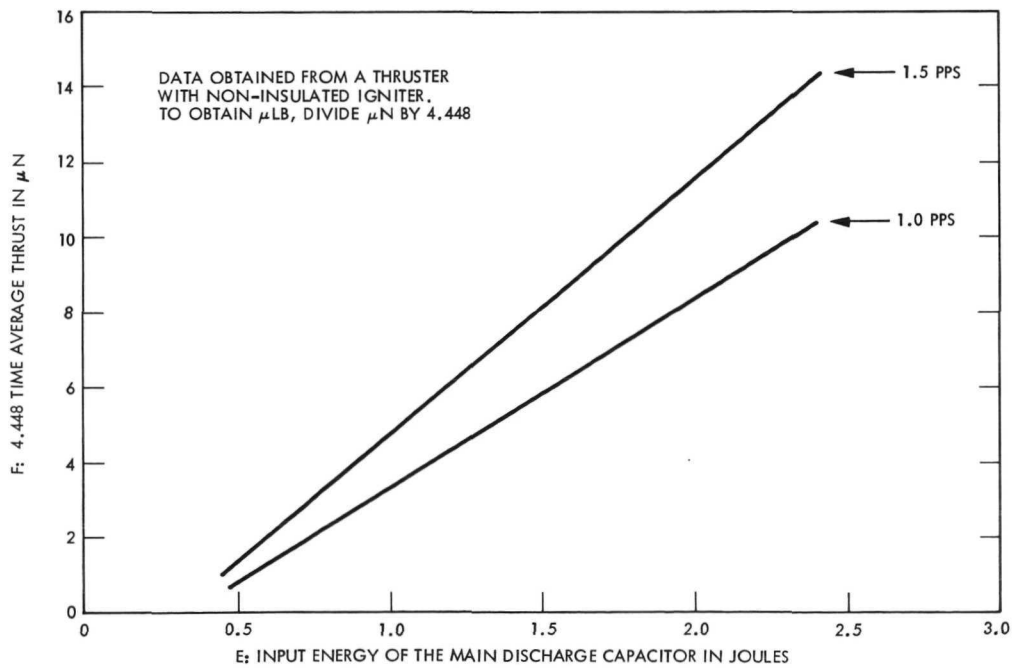Fig. 9. Comparative time average vs ignition command rate

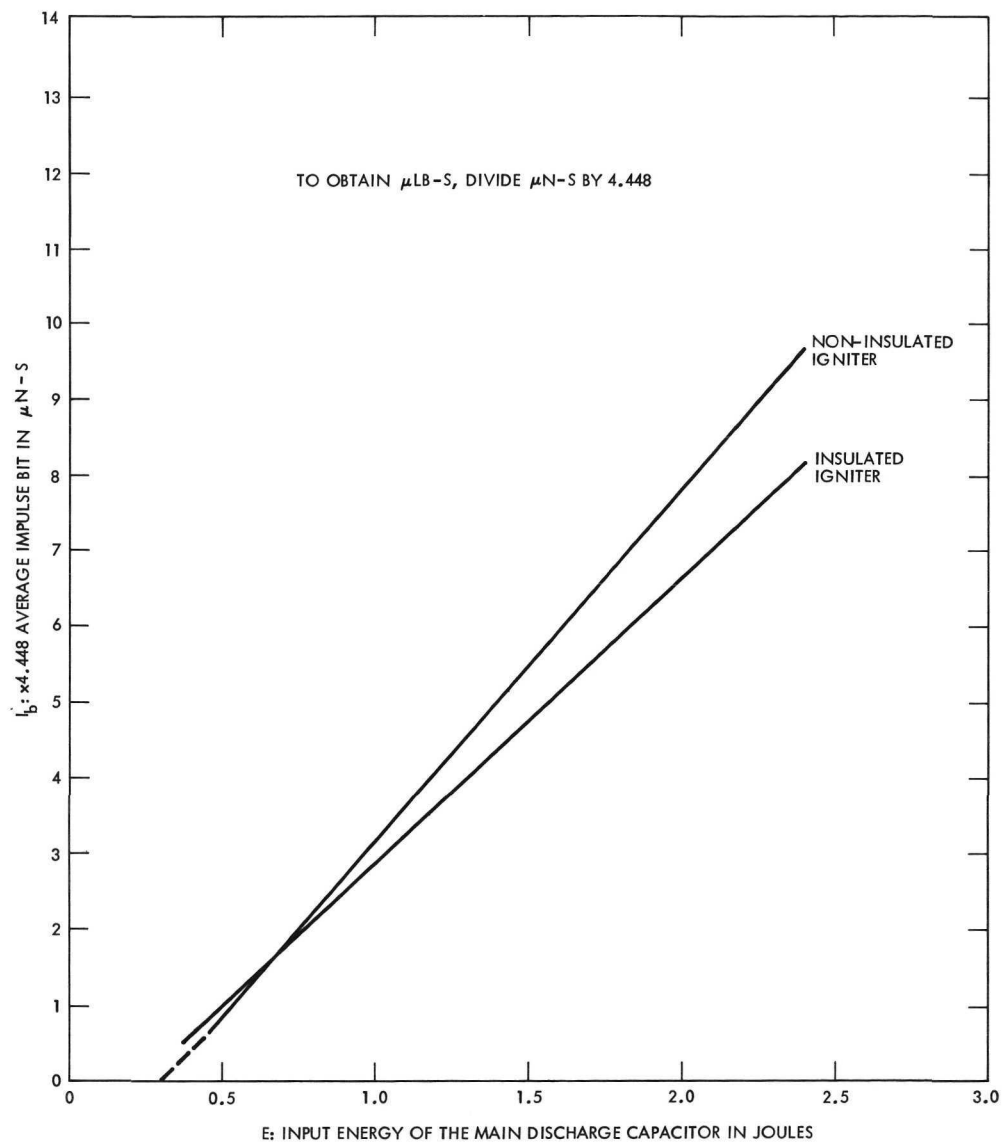Fig. 10. Time average thrust vs input energy
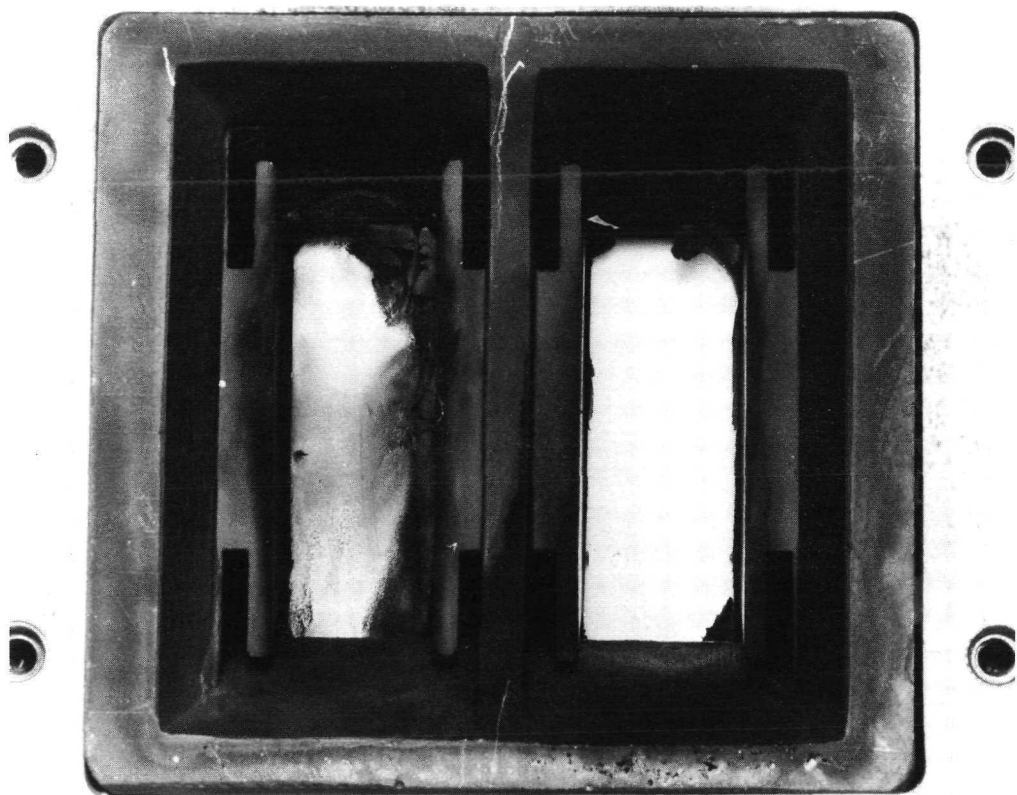
Fig. 11. Comparative average impulse bit vs input energy

Fig. 12. Front view of the propellant and the igniter assembly of the LES-6 thruster

Fig. 14. Closeup view of the igniter surface of the thruster with noninsulated igniter and after approximately 100,000 accumulative ignitions (input voltage = 1500 V dc)
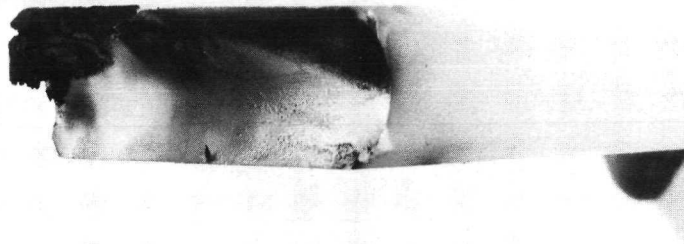

Fig. 13. Closeup view of the igniter surface, with proper insulation and after 300,000 accumulative ignitions (input voltage = 1500 V dc)

Fig. 15. Photograph of the Teflon bar from the thruster with noninsulated igniter and after 10^5 accumulative ignitions (input voltage = 1500 V dc)
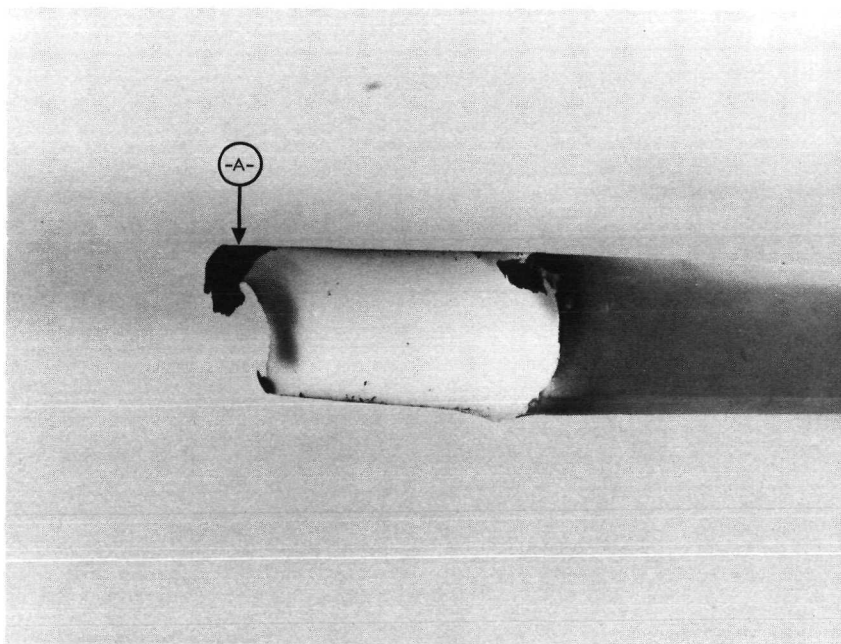

Fig. 16. Photograph of the Teflon bar from the thruster with insulated igniter and after 3×10^5 accumulative ignitions (input voltage = 1500 V dc)
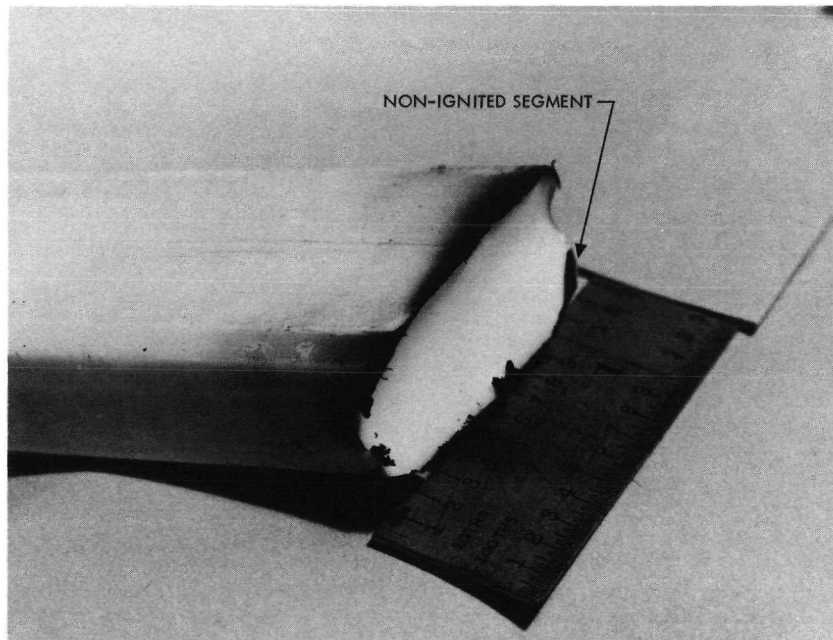
Fig. 17. Photograph of the Teflon bar with insulated
and clean igniter and after 150,000 accumulative
ignitions (area = 3.26 cm^2 or 0.505 in.^{2})(input
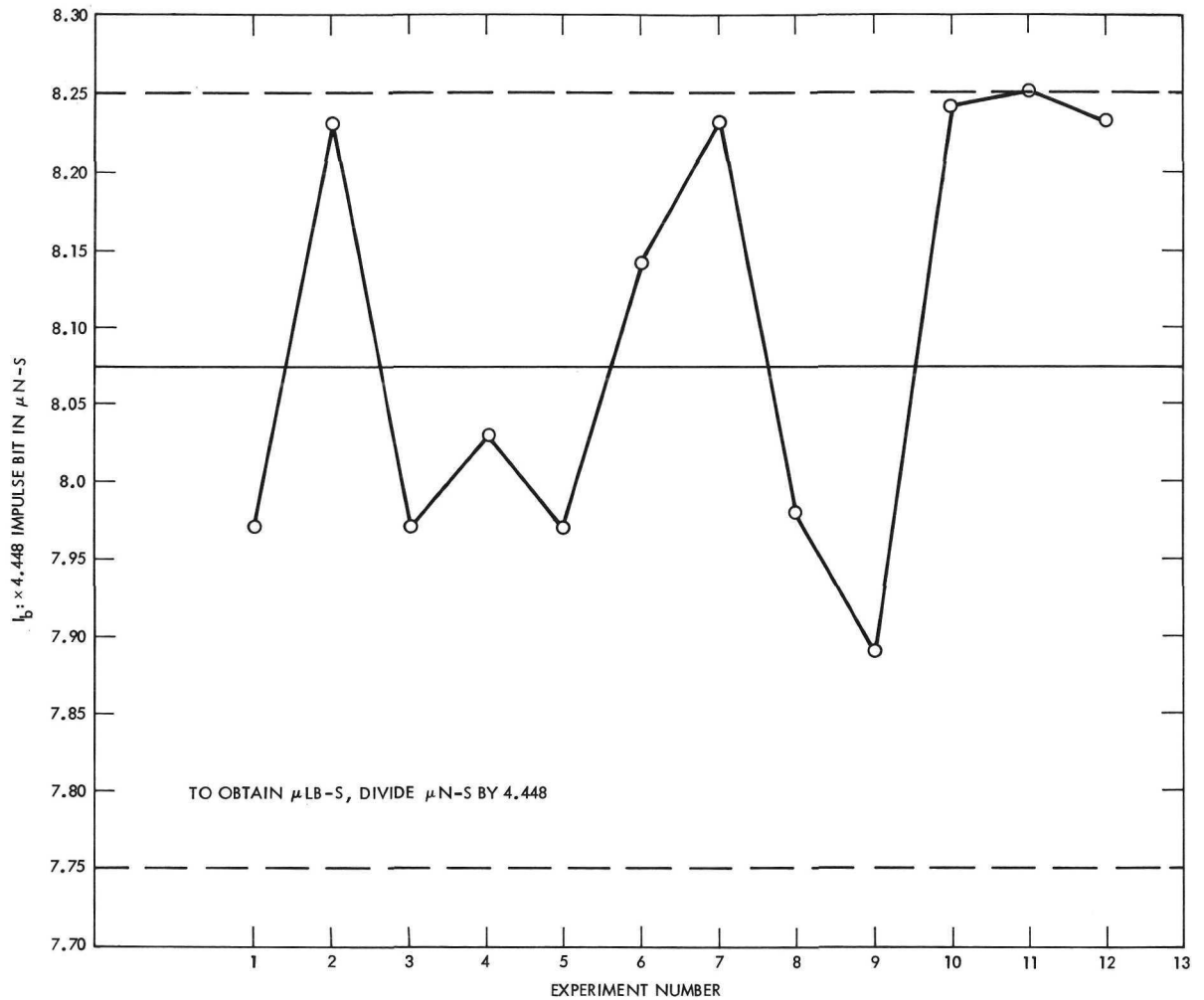voltage = 1500 V. dc)

Fig. 18. Impulse bit repeatability with constant input energy (2.25 joules), constant igniter resistance (3.5 ohms), and constant frontal area of Teflon bar (3.26 cm^2 or 0.505 in.^{2})
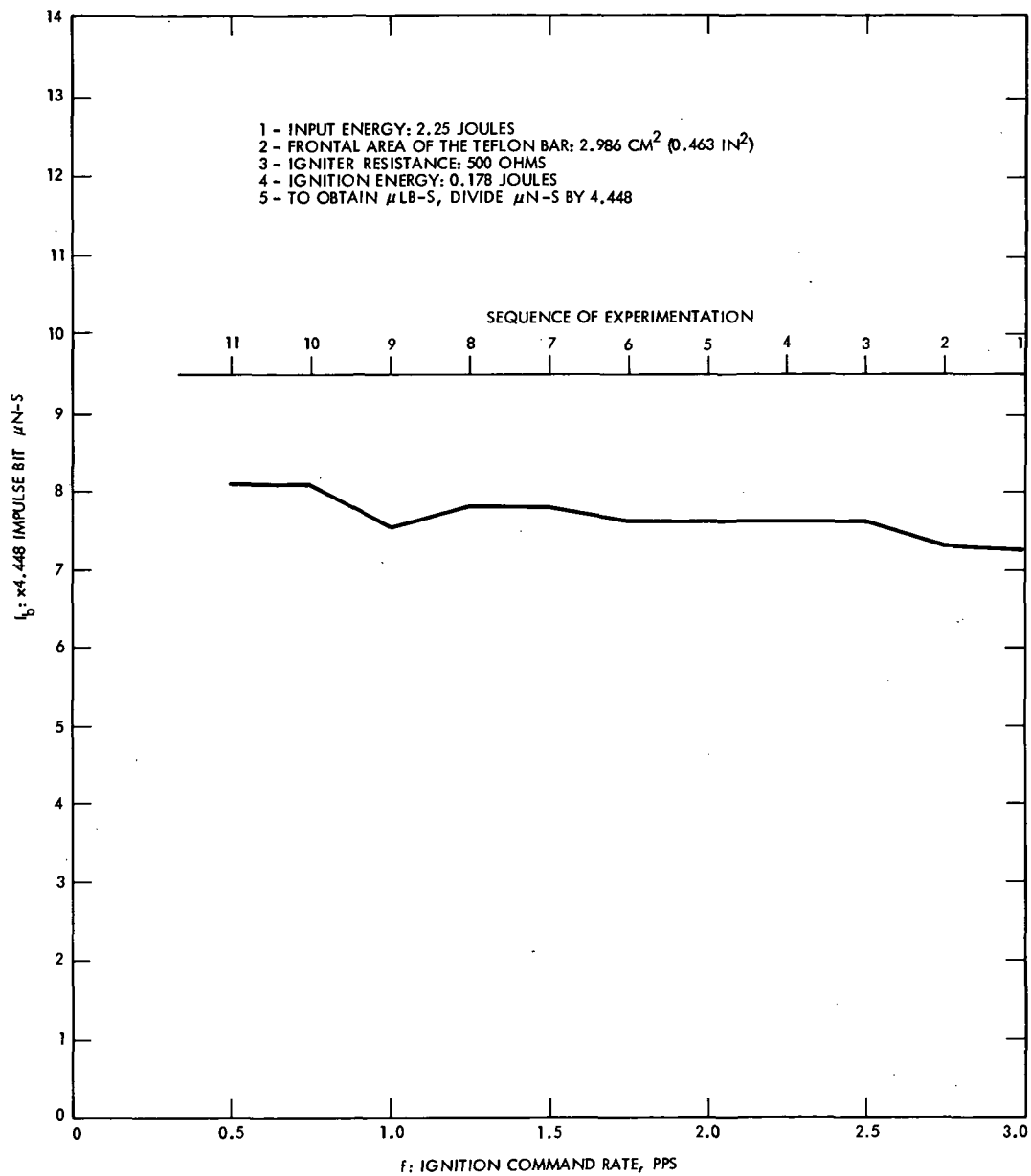
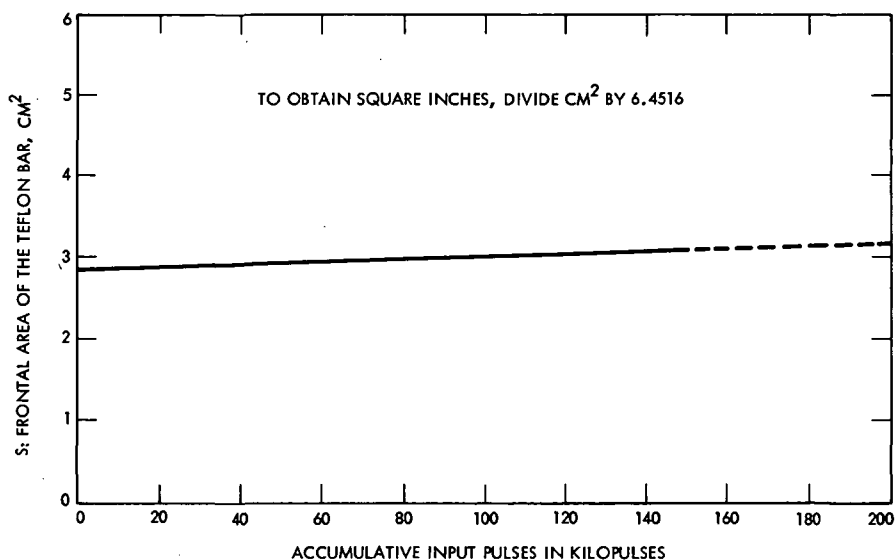Fig. 19. Impulse bit vs ignition command rate at constant input energy

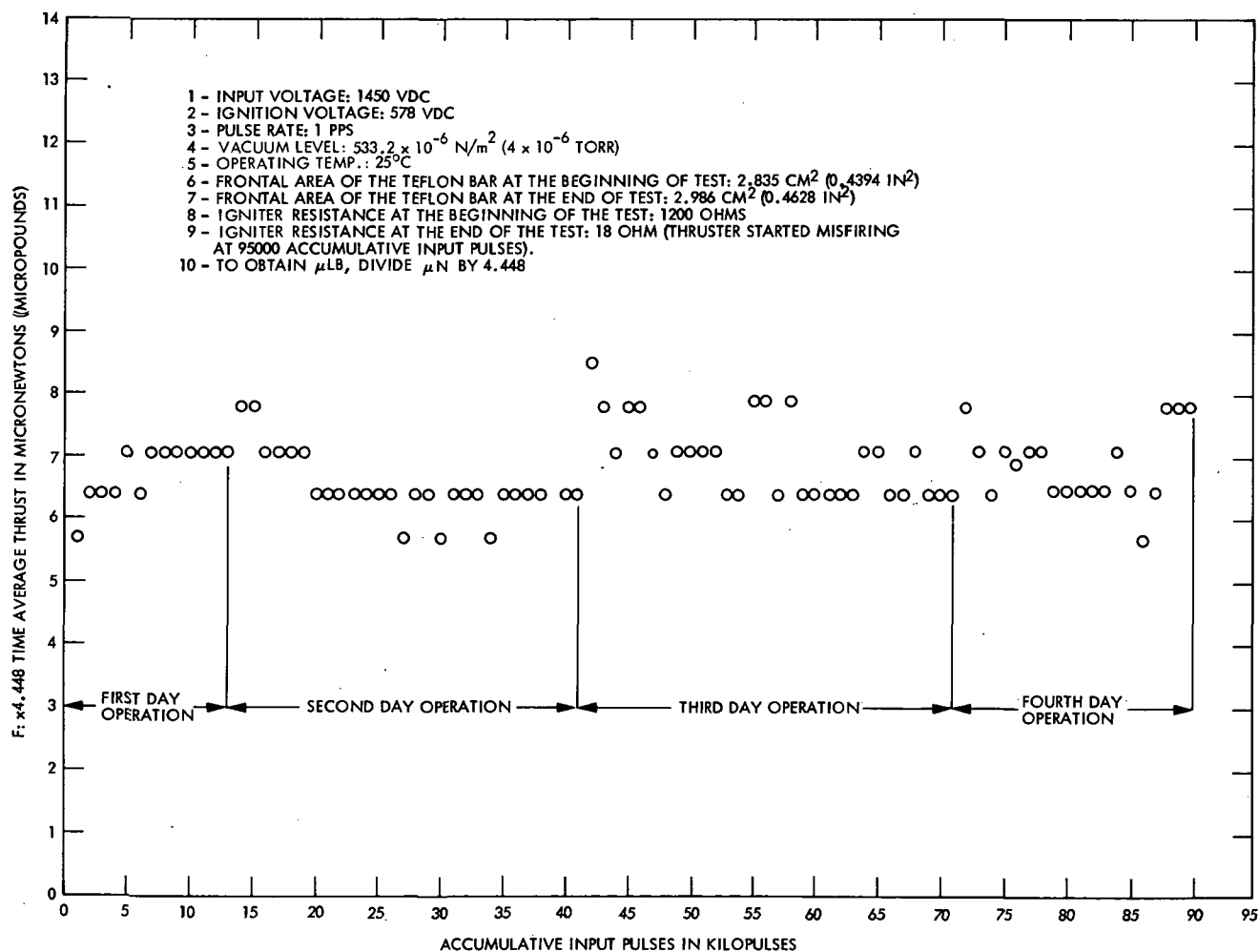Fig. 20. Accumulative input pulses vs frontal area of the Teflon bar

Fig. 21. Time average thrust vs accumulative input pulses
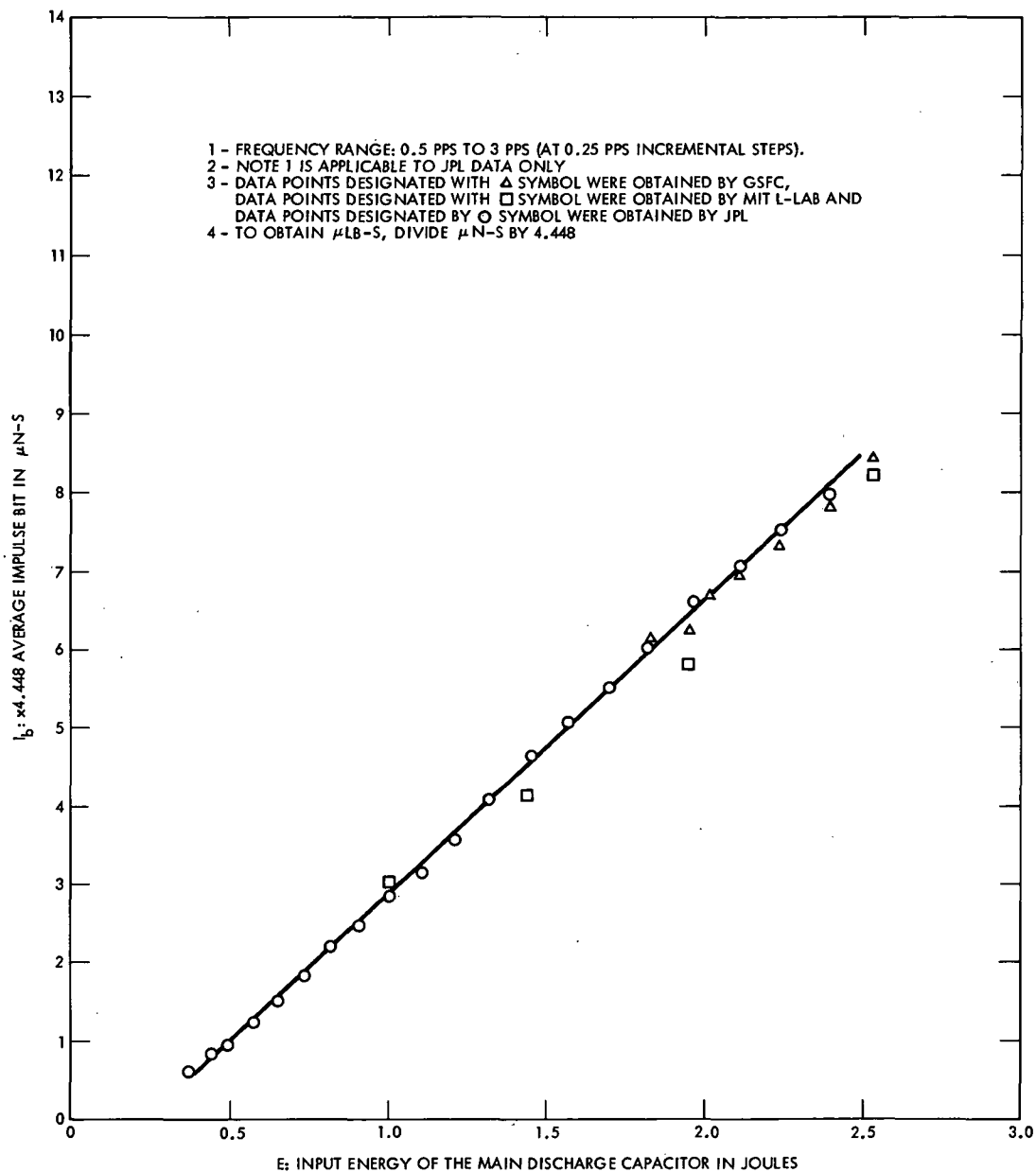
Fig. 22. Comparative average impulse bit vs input energy
obtained by GSFC, MIT, and JPL

APPENDIX A

Thruster Diagrams and Calibration Data

Table A-1. Strain data of 0.41 mm (16 mil) stainless steel wire torsion wire

Load kg (lbs)	Length cm (Inches)
0 (0)	27.94 (11)
2.268 (5)	28.008 (11.027)
4.535 (10)	28.052 (11.044)
6.803 (15)	28.100 (11.063)
9.07 (20)	28.163 (11.088)
13.605 (30)	28.397 (11.180)
18.14 (40)	28.671 (11.288)
18.59 ≃(41)	*

*At the designated load wire was fractured.

Table A-2. Period of oscillation of pendulum with standard inertia disk

| Period Number	Period of Oscillation of System Under Vacuum Level of 133.3×10^{-5} N/m^2 (10^{-5} torr), sec
1	43.63
2	42.78
3	43.58
4	44.00
5	42.10
6	43.28
7	43.10
8	42.76
9	42.87
10	43.32
Average	43.26

Table A-3. Photo sensor calibration at ambient illumination

Angular Displacement in Arc Minutes	Output of Photo Cells in mV	Angular Displacement in Arc Minutes	Output of Photo Cells in mV	Angular Displacement in Arc Minutes	Output of Photo Cells in mV
0	1.09	440	5.43	880	10.14
20	1.27	460	5.66	900	10.36
40	1.46	480	5.87	920	10.57
60	1.64	500	6.09	940	10.76
80	1.81	520	6.28	960	10.92
100	1.99	540	6.47	980	11.00
120	2.17	560	6.68	1000	11.02
140	2.36	580	6.91	1020	11.02
160	2.56	600	7.15	1040	11.03
180	2.76	620	7.38	1060	11.03
200	2.96	640	7.59	1080	11.03
220	3.17	660	7.82	1100	11.03
240	3.38	680	8.07		
260	3.58	700	8.29		
280	3.78	720	8.50		
300	3.97	740	8.70		
320	4.15	760	8.87		
340	4.34	780	9.08		
360	4.56	800	9.28		
380	4.78	820	9.51		
400	4.99	840	9.73		
420	5.20	860	9.93		

An optical dividing head was employed in this experiment.

The geometry of the shadow bar and the moment arm of the pendulum's platform was duplicated in this experiment.

Exact number of cells (one) were uncovered as in the actual system.

Direction of rotation cw.

Irradiant power of the photo cells was supplied by both the light source of the pendulum system and the room lighting.

Table A-4. Photo sensor calibration under the bell jar of the vacuum system

Total Angular Displacement Degrees	Total Output in mV	Millivolt Output per Arc Minute Displacement
1.5	0.55	6.12×10^{-2}
1.5	0.55	6.12×10^{-2}
1.5	0.56	6.22×10^{-2}
1.5	0.58	6.45×10^{-2}
1.5	0.57	6.34×10^{-2}
Average over 1.5 deg	0.5625	6.25×10^{-2}
3.5	0.140	6.67×10^{-2}
3.5	0.134	6.28×10^{-2}
3.5	0.137	6.52×10^{-2}
3.5	0.133	6.32×10^{-2}
3.5	0.135	6.43×10^{-2}
Average over 3 deg	0.1358	6.465×10^{-2}

This experiment was conducted with the actual system. The angular displacement of the platform was achieved by magnetic coupling (controlled externally).

A digital voltmeter along with the pendulum system's protractor were used to measure output voltages and the displacement angles of the platform.

$$\text{Photo Sensor Scale Factor} = \frac{10^{-2}(6.465 + 6.25)}{2}$$

$$= 6.357 \times 10^{-2} \text{mV/Min}$$

Fig. A-1. Trigger generating network
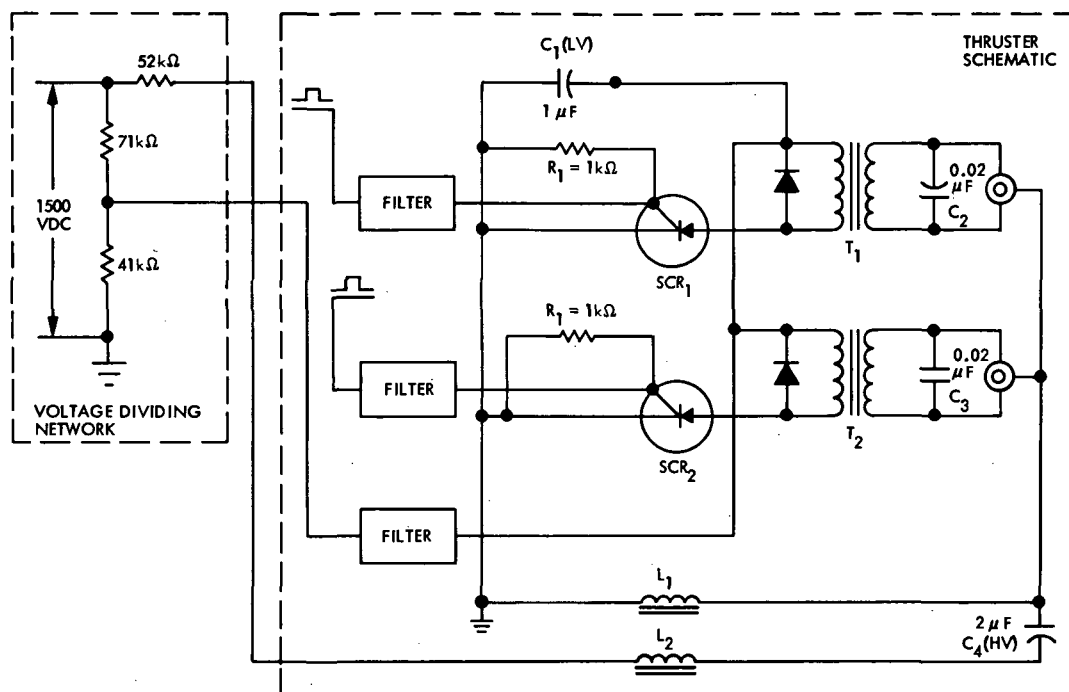

Fig. A-2. Lamp drive circuit
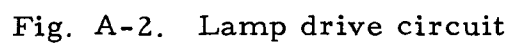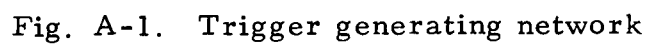
Fig. A-3. Voltage-dividing network and thruster schematic
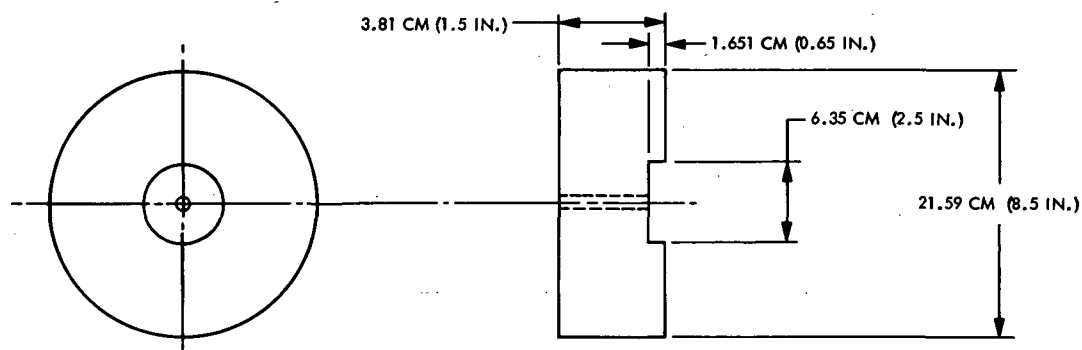

Fig. A-4. Standard inertia disk (material, Al; weight = 3.719 kg or 8.2 lb)

APPENDIX B

Test Equipment and its Characteristics

Table B-1. Test equipment and its characteristics

Description	Range	Manufacturer and Part Number	Quantity
Pulse Generator	Range $\begin{cases}10^{-4} - 100 \\ 1K - 100K\end{cases}$ Functions $\begin{cases}\text{Square} \\ \text{Pulse} \\ \text{Sine} \\ \text{Ramp} \\ \text{Triangular}\end{cases}$	Hewlett Packard Function Generator 3310A	
D.C. Power Supply, Ignition Command or Optical Coupler	0-50 VDC, 5 Amps 0-25 VDC, 1 Amp	Hewlett Packard Harrison 6220B	1
Digital Voltmeter	1-10K-Ohms 1-1000 Volts AC 10-1000 Volts DC 100-1000 Millivolts DC	Non-Linear Systems Inc. Series X-2	1
D.C. Power Supply, Photo-Readout Assy.	0-60 VDC 0-2.4 Amps Regulated	Lambda Electronics LH-128 AFM	1
High Vacuum System	Mechanical Pump: 42.5 cm^3/min (15 ft^3/min) Diffusion Capacity: 2000 dm^3/sec (70.7 ft^3/sec) Bell Jar Size: 45.72 cm x 76.2 cm (18" x 30") Vacuum Level: 133.3 x 10^{-8} N/m^2 (1 x 10^{-8} Torr)	Veeco 775	1
High Voltage Power Supply	0-4 Kilovolts 0-50 Milliamperes	Hewlett Packard, Harrison 6525 A	1
Accumulative Mech- anical Output Counter	0-7 x 10^6 Counts		
D.C. Power Supply, Mechanical Counter.	0-50 VDC 0-1.5 Amps	Power Designs 5015A	1
X-Y Plotter	X-Axis 0.039-19.69* (0.1-50**) Y-Axis 0.039-19.69* (0.1-50**) *Division per cm **Division per inch sensitivity Rate: 0.025-5.08 cm/sec (0.01-2 inch/sec)	Honeywell 520 X-Y Reorder	1
Frequency Counter	Time Base $\begin{cases}0.1 \ \mu sec \\ \text{to } 10^9 \ sec\end{cases}$ Double $\begin{cases}\text{Attenuation} \\ \text{X1 to X100}\end{cases}$ Channel	Hewlett Packard 5325B Universal	1
Accumulative Input Pulse Counter	Sensitivity: 0.1-10 V-RMS Frequency: (0.01-10 KC) Time Count Sec. Periods: 1-100K, Micro-Sec	Hewlett Packard 5532A Electronics	1
Oscilloscope, Storage	Volts/Div.: 0.01-20 Time/Div. $\begin{cases}0.5\text{-}50 \ \mu sec/ \\ 0.1\text{-}50 \ msec/ \\ 0.1\text{-}1 \ \ sec/\end{cases}$ Calibration Scale: 0.2 mv-50 mv 0.1 V - 100V	Tektronix Inc. Type 564 Time Base: Type 383 Dual Trace: Type 3A72	1
Torsion Pendulum	Torsion wire 0.41 mm (16 mil) K=8.05 μN-m/deg (5.915 lb-ft/deg) Standard Inertia: 2.182 x 10^{-2}kg-m^2 (1.609 x 10^{-2} slug-ft^2)	General Electric Spacecraft Dept. S/N TP-3	1